### Title

Unified Structural Representation of the southern California crust and upper mantle




### Authors

Shaw, John H
Plesch, Andreas
Tape, Carl
et al.



### Publication Date

2015-04-01

### DOI

10.1016/j.epsl.2015.01.016

Peer reviewed

# Unified Structural Representation of the southern California crust and upper mantle

Authors
John H. Shaw[1], Andreas Plesch[1], Carl Tape[1,2], M. Peter Suess[3], Thomas H. Jordan[4], Geoffrey Ely[4], Egill Hauksson[5], Jeroen Tromp[6], Toshiro Tanimoto[7], Robert Graves[8], Kim Olsen[9], Craig Nicholson[10], Philip J. Maechling[4], Carlos Rivero[11], Peter Lovely[12], Charles M. Brankman[13], and Jason Munster[14]

[1]Department of Earth & Planetary Sciences, Harvard University, 20 Oxford St., Cambridge, MA, USA, 02138 // shaw@eps.harvard.edu // 617 495-8008

[2]University of Alaska Fairbanks, Geophysical Institute, 903 Koyukuk Drive, Fairbanks, AK, USA, 99775-7320

[3]Department of Geosciences, Tübingen University, Hölderlinstr. 12, 72074 Tübingen, Germany

[4]Southern California Earthquake Center, University of Southern California, Los Angeles, CA, USA, 90089-0742

[5]Division of Geological and Planetary Sciences, Seismological Laboratory, California Institute of Technology, Pasadena, CA, USA , 91125

[6]Department of Geosciences, Princeton University, Guyot Hall, Princeton, NJ, USA, 08544

[7]Department of Earth Science , 1006 Webb Hall , University of California Santa Barbara, CA, USA, 93106-9630

[8]U.S. Geological Survey 525 South Wilson Avenue Pasadena, CA, USA, 91106

[9]Dept. Geological Sciences, MC-1020, 5500 Campanile Dr., San Diego State University, San Diego, CA, USA, 92182-1020

[10]Marine Science Institute. University of California, Santa Barbara, CA, USA, 93106-6150

[11]Chevron North America E&P, Gulf of Mexico Regional Team, Houston, TX, USA, 77002

[12]Chevron ETC – ESD, 1500 Louisiana, 28077, Houston, TX, USA, 77002

[13]IHRDC, 535 Boylston Street, Boston, MA, USA, 02116

[14]School of Engineering and Applied Sciences, Harvard University, 29 Oxford St., Cambridge, MA, USA, 02138

**Abstract**

We present a new, 3D description of crust and upper mantle velocity structure in southern California implemented as a Unified Structural Representation (USR). The USR is comprised of detailed basin velocity descriptions that are based on tens of thousands of direct velocity (Vp, Vs) measurements and incorporates the locations and displacement of major fault zones that influence basin structure. These basin descriptions were used to developed tomographic models of crust and upper mantle velocity and density structure, which were subsequently iterated and improved using 3D waveform adjoint tomography. A geotechnical layer (GTL) based on Vs30 measurements and consistent with the underlying velocity descriptions was also developed as an optional model component. The resulting model provides a detailed description of the structure of the southern California crust and upper mantle that reflects the complex tectonic history of the region. The crust thickens eastward as Moho depth varies from 10 to 40 km reflecting the transition from oceanic to continental crust. Deep sedimentary basins and underlying areas of thin crust reflect Neogene extensional tectonics overprinted by transpressional deformation and rapid sediment deposition since the late Pliocene. To illustrate the impact of this complex structure on strong ground motion forecasting, we simulate rupture of a proposed M 7.9 earthquake source in the Western Transverse Ranges. The results show distinct basin amplification and focusing of energy that reflects crustal structure described by the USR that is not captured by simpler velocity descriptions. We anticipate that the USR will be useful for a broad range of simulation and modeling efforts, including strong ground motion forecasting, dynamic rupture simulations, and fault system modeling. The USR is available through the Southern California Earthquake Center (SCEC) website (www.scec.org).

Key words: velocity structure; fault models; southern California; tomography; seismic wave propagation; strong ground motions

Acknowledgements: This work was supported by the Southern California Earthquake Center, the National Science Foundation, and the U.S. Geological Survey. SCEC is funded by NSF Cooperative Agreement EAR-1033462 and USGS Cooperative Agreement G12AC20038. This work was also supported through NSF awards EAR-1226343 titled “Geoinformatics: Community Computational Platforms for Developing Three-Dimensional Models of Earth Structure” and EAR-1349180 titled “Community Computational Platforms for Developing Three-Dimensional Models of Earth Structure, Phase II.” The SCEC contribution number for this paper is 2068.

## 1. Introduction

Recent advances in numerical methods and parallel computing technology have enabled large-scale 3D simulations of seismic wavefields in realistic earth models [e.g., Olsen et al., 1995; Komatitsch & Tromp, 1999; Komatitsch et al., 2004; Bielak et al., 2010]. These simulations are able to capture the effects of basin amplification, resonance, wave focusing, and dynamic rupture propagation. Thus, they offer a physics-based alternative to attenuation relationships (e.g., Abrahamson and Silva, 1997; 2008; Field, 2000; Boore and Atkinson, 2008) for forecasting the distribution of hazardous ground shaking during large earthquakes (e.g., Zhao et al., 2000; Tromp et al., 2005; Tromp et al., 2005; Tarantola, 1984; Chen et al., 2007). These methods also provide an objective, quantitative means of using seismic observations to improve 3D earth models. The revised models, in turn, help make strong ground motion forecasts more accurate.

To facilitate these and other studies, we present a Unified Structural Representation (USR) of southern California (Fig. 1). The USR consists of two major components: a 3D description of seismic wavespeeds (Vp, Vs) and density ($\rho$), known as a community velocity model (CVM); and a 3D description of the major fault systems in the region, known as a community fault model (CFM). The CVM includes a framework of geologic horizons that define the various rock units in the region and integrates a wide range of direct observations that define velocity structure. These include tens of thousands of velocity measurements in boreholes, as well as constraints from seismic reflection and refraction studies in sedimentary basins. The basin structures are used to develop travel time tomographic models of the crust and upper mantle extending to a depth of 33 km, and a teleseismic shear wave model of the upper mantle to a depth of 150 km. This combined velocity model was then subjected to a series of 3D adjoint tomographic inversions that highlight areas of the starting model that were responsible for mismatches between observed and synthetic waveforms (Tape et al, 2009; 2010). Sixteen tomographic iterations, requiring 6,800 fully 3D wavefield simulations, yielded perturbations to the starting model that have been incorporated into the current CVM. The second component of the USR is the CFM, which provides 3D descriptions of the major fault systems in southern California that are considered to pose earthquake hazards. These 3D fault representations are defined by surface geology, earthquake hypocentral locations, focal mechanisms, well, and seismic reflection data. The USR provides compatible fault and velocity models, in which the locations and displacements of major faults are explicitly represented in the velocity descriptions.

## 2. Tectonic history and structure

Southern California sits astride a tectonic plate boundary that has been active for at least 200 million years. Beginning in the Jurassic Period, subduction of oceanic crust beneath

North America created the Sierra Nevada arc and associated igneous terrains, a widespread series of forearc deposits including the Great Valley sequence, and the Franciscan accretionary complex, which is exposed in the Coast Ranges (e.g., Hamilton, 1969; Ernst, 1970; Dickinson, 1981; Cowan and Bruhn, 1992). These north-south trending elements define the primary tectonic fabric and bedrock geology of the state (Fig. 2). In southern California, these features have been displaced and overprinted by two Tertiary tectonic events. In the Neogene, parts of the southern California continental lithosphere were captured by the Pacific plate and moved obliquely away from North America (Nicholson et al., 1994). This motion led to the clockwise rotation of the Transverse Ranges (Luyendyk et al., 1985; Kamerling and Luyendyk, 1985; Hornafius et al., 1986), the opening of the Inner California Continental Borderland, and development of a series of deep sedimentary basins along the southern California coast (Crouch and Suppe, 1993). In the Pliocene, seafloor spreading in the Gulf of California and development of the modern San Andreas transform system (Hill and Dibblee, 1953; Atwater, 1970; Allen, 1981; Curray and Moore, 1984) led to a transpressional tectonic regime (Zoback et al., 1987) that further displaced and locally reactivated the earlier rift and subduction zone structures. This tectonic regime drives present-day deformation of the southern California lithosphere (Minster and Jordan, 1978; Bird and Rosenstock, 1984; Humphreys and Hager, 1990; Meade and Hager, 2005), and is characterized by right-lateral strike-slip motion on the San Andreas, San Jacinto, Eastern California Shear Zone, and other major northwest trending fault systems (Fig. 2). The Salton Trough has developed as a result of oblique rifting of Baja California away from Sonora Mexico and subsequent transfer of slip from the Imperial to the southern San Andreas fault, forming a pull-apart basin (Rockwell and Sylvester, 1979). Farther north, a major restraining bend in the San Andreas fault drives active deformation within the Transverse Ranges (Fig. 2), which is characterized by thrust and oblique reverse faulting (Reed and

Hollister, 1936; Namson and Davis, 1988; Yeats, 1988; Yeats et al., 1988; Shaw and Suppe, 1994). In the eastern part of the state, the crust is also being actively deformed by Basin and Range extensional tectonics (Wernicke at al., 1988; Burchfiel et al., 1987), which accommodates a component of Pacific and North American relative plate velocity (Minster and Jordan, 1978; DeMets et al., 1987). The Garlock fault, an active left-lateral strike slip system (Smith 1962; 1975; Smith and Ketner, 1970; Astiz and Allen, 1983; McGill and Sieh, 1993), defines the southern boundary of this Basin and Range extensional province and separates it from the Mojave region (Minster and Jordan, 1987). The Mojave region is characterized by dextral slip on faults that comprise the Eastern California Shear Zone (Dokka and Travis, 1990; Savage et al., 1990).

This complex tectonic history is manifest in the geologic and geophysical structure of the southern California crust and upper mantle. The depth of the crust, defined by the Mohorovičić discontinuity, changes abruptly from about 10 km in the Pacific Plate to about 20 km in the continental shelf (Fig. 3). The crust generally continues to thicken eastward, with the Moho reaching a maximum depth of about 40 km (Yan and Clayton, 2007; Tape et al., 2012). In central California, this eastward thickening reflects the transition from oceanic crust, through the Franciscan assemblage, the forearc sequence of the Great Valley, to the thick crustal roots of the Sierra Nevada arc. This pattern is made complex in southern California by the rotation and translation of the Western Transverse Ranges that unroofed the Inner California Borderland during the Neogene. Crustal thickness has also been affected by the Pliocene and Quaternary deepening of the coastal basins and formation of the Salton Trough along the southern San Andreas fault system. As a result, the crust is thickest (35 – 40 km) beneath the Transverse and Peninsular Ranges and thinnest ( ≈ 20 km) beneath the coastal basins.

The stratigraphy and composition of the crust in southern California also reflects this region's tectonic history. Mesozoic to early Tertiary deposits are generally part of the forearc system, yet they have been dissected and displaced by Neogene and younger deformations. Neogene deposits are widespread in southern California, with the thickest accumulations occurring in rift and subsequently transpressional basins that formed in response to microplate capture, rotation of the Transverse Ranges, and opening of the Inner California Borderland (Nicholson et al., 1994; Crouch and Suppe, 1993). Thick Pliocene and younger deposits are localized in coastal basins such as Ventura and Los Angeles (Fig. 2) that continued to subside as a result of sedimentary and tectonic loading (Yerkes et al., 1987; Wright, 1991; Namson and Davis, 1988; Shaw and Suppe, 1994).

The seismic wavespeed structure in southern California reflects this complex geologic history. In order to represent this structure accurately, we need to generate consistent representations of faults and basins, and to incorporate a variety of different types of data and models in a self-consistent manner. We term this a Unified Structural Representation, and describe in the following section how it was constructed.

## 3. Development of a Unified Structural Representation

The USR incorporates a variety of different velocity constraints, ranging in resolution from 10-cm-scale borehole observations in shallow sedimentary sections to 3D tomographic models that describe the upper mantle at scales of tens of kilometers. These components must be assembled in a way that ensures their internal consistency. Thus, we developed a workflow for building the USR that begins with the development of structural representations of the basins and parameterization of their internal velocity structures, including gradients associated with major faults. These basin models are

187 then used as input for the development of tomographic models of the crust and upper
188 mantle. Integrated basin and tomographic models were subsequently evaluated and
189 improved using 3D, adjoint waveform tomographic methods. Finally, a geotechnical layer
190 based on Vs30 measurements was developed as an optional overprint to facilitate the
191 model's use in strong ground motion studies and engineering applications. The following
192 sections describe the development of each of these model components.
193
194 **3.1 Basin structures**
195 Deep sedimentary basins in southern California form significant velocity structures in the
196 crust. These basins are generally filled with thick (> 10 km) sequences of relatively low
197 velocity and density sediments that have been shown to amplify seismic waves and
198 localize hazardous ground shaking during large earthquakes (e.g., Bonamassa and
199 Vidale, 1991; Frankel and Vidale, 1992; Bouchon and Barker, 1996; Olsen, 2000;
200 Graves et al., 1998; Bielak et al., 1999; Aagaard et al., 2001; Komatitisch et al., 2004;
201 Minster et al., 2004; Graves et al., 2011). Thus, the first step in our development of the
202 USR was to generate accurate descriptions of the 3D geometry and velocity structures
203 of the major basins.
204
205 The initial step in representing basin structures was to identify stratigraphic horizons or
206 surfaces that define the extent of basins or represent abrupt changes in velocities or
207 velocity gradients. An analysis of our borehole data shows that several lithologic markers
208 represent significant, laterally continuous velocity and density boundaries in the basins.
209 The most important of these is the transition from sedimentary to basement rocks, which
210 defines a major velocity discontinuity throughout most of southern California (Fig. 4).
211 This sediment-basement boundary defines the depth and extent of the basins, and
212 represents juxtaposition of different rock types and ages in various parts of the crust. In

213 the western Los Angeles basin, the California Borderland, and the Santa Barbara basin
214 the sediments are generally underlain by Catalina schist and other metamorphic rocks
215 that are part of the Franciscan subduction zone complex. In the eastern Los Angeles
216 and San Bernardino basins the basement is generally formed by igneous rocks (Wright,
217 1991; Crouch and Suppe, 1993). In the Ventura, Santa Maria, and Salton Trough basins,
218 the basement surface represents a transition from Neogene and younger sedimentary
219 rocks to early Tertiary and Mesozoic metasedimentary sequences (Fuis and Kohler,
220 1984; Yerkes et al., 1987; Brankman, 2009; Namson and Davis; 1990; Lovely et al.,
221 2006). In the Ventura and Santa Maria basins this boundary generally represents a
222 distinct disconformity, whereas in the Salton Trough the top of basement likely
223 represents a geothermal boundary that reflects the high present-day crustal heat flow in
224 the region.
225
226 The depth and shape of the basement surface are highly variable across southern
227 California, ranging from surface outcrops along the basin edges to depths of more than
228 10 km in Ventura and Los Angeles (Fig. 1B). Surface outcrops of the basement surface
229 were digitized from the California State geologic map (Jennings et al., 1977) with more
230 local detail added based on the Dibble Map Series (e.g., Dibble, 2005). The subsurface
231 location of the basement surface is defined directly by two primary types of data (Fig. 4).
232 The first are well penetrations, generally acquired by the petroleum or geotechnical
233 industries, which use cuttings and/or electric logs to define this lithologic boundary.
234 Dozens of wells in the western Los Angeles, Ventura, and Santa Maria basins, and in
235 the Inner California Borderland directly penetrate this horizon and are used as direct
236 constraints on basin depth and shape (see Wright, 1991). The second type of constraint
237 on the basement surface is provided by seismic reflection data. The petroleum industry
238 has acquired tens of thousands of line kilometers of 2D seismic reflection profiles and

several 3D surveys in the southern California coastal basins and offshore. As the sediment-basement interface generally represents an abrupt velocity contrast, it is often imaged by a prominent reflector in these data (e.g., Legg and Nicholson, 1993; Shaw and Suppe, 1994; Bohannon and Geist, 1998; Rivero et al., 2011). The quality of the data, as well as the depth and magnitude of the impedance contrast across the surface, controls the character of this reflection and our ability to map it precisely. The basement reflector is best defined in surveys from the western Los Angles basin, the California Borderland, and Santa Barbara basin. Moreover, the reflector is tied directly to well penetrations throughout these regions. Together, these surface geologic, well, and seismic reflection constraints define the basement surface throughout much of southern California. In areas where the basement is not directly defined, geologic cross sections (e.g., Namson and Davis, 1988; 1990; Shaw and Suppe, 1994, 1996; Huftile and Yeats, 1995; Tsutsumi et al., 2001) and potential field studies (e.g., McCulloh, 1960) provide further estimates that help us generate a continuous basement surface (Fig. 1).

The shapes and velocity structures of the sedimentary basins in southern California are influenced significantly by the locations and displacement of major fault systems. The southern California crust contains more than 150 active faults that are deemed capable of generating moderate to large magnitude earthquakes (Plesch et al., 2007), as well as many other structures that were active in earlier tectonic periods (Fig. 1C). Neogene-age normal and strike-slip faults that accommodated rotation of the Western Transverse Ranges and opening of the Inner California Borderland localized the development of the major coastal basins (Luyendyk et al., 1985; Hornafius et al., 1986; Crouch and Suppe, 1993; Nicholson et al., 1994). As such, these faults often bound basins and are related to many internal basin structures that influence basin shapes. Moreover, Pliocene and younger faulting has displaced the basement surface in many locations, producing

abrupt lateral contrasts in velocity between rocks and sediments. Thrust and reverse faults have, in some cases, displaced the basement over stratigraphic units leading to velocity inversions (i.e., downward decreases in velocity). These velocity inversions have been shown to be important in wave focusing and amplification (e.g., Graves et al., 1998), and thus it is important to represent them in models that are used for strong ground motion simulations.

To represent these faults in our basin structures, we developed in parallel a comprehensive 3D fault model (SCEC Community Fault Model [CFM]; see Plesch et al., 2007). This model represents faults as triangulated surface representations (tsurfs) that are defined by wells, seismic reflection profiles, geologic cross sections, earthquake hypocentral locations (e.g., Shearer et al., 2005; Lin et al., 2007), and focal mechanism solutions (Yang et al., 2012) (Fig. 1C). We use a subset of these fault representations, along with other faults that are no longer active and thus not included in the CFM, to help define our representations of the Los Angeles, Ventura, Santa Barbara, and Santa Maria basins. We included faults that had significant total displacements in two ways. Those that bounded the basins were used to model the shape of the basement horizon. Others were used to offset the basement surface (see Fig. 5).

Once the sedimentary basin volumes are defined by topography, bathymetry, and the basement surface, we parameterize the internal basin velocity structure. Direct measurements of seismic velocities are provided by several different types of observations. Velocities are recorded by sonic logs, which are wireline tools passed along a borehole that measure interval transit times between pairs of sound sources and receivers. These transit times are readily converted into interval velocities (Fig. 4). Most sonic logs measure only Vp; however, dipole sonics acquired by the energy industry and

suspension logs in the geotechnical industry can evaluate both Vp and Vs. Active source experiments, including seismic refraction and reflection surveys, also provide estimates of seismic velocity. These data have been acquired in many of the southern California basins, and are most abundant in coastal and offshore basins that have been explored by the petroleum industry. In addition, industry reflection data typically provide stacking velocities, which can be converted to interval velocities. While these derived velocities are far less precise than those from sonic logs, they offer the advantage of broad coverage across basins and generally constrain velocities at depths that are greater than most well penetrations.

Based on these observations, previous velocity models in southern California have used several different approaches to parameterize sediment velocities. Magistrale et al. (2000) used a rule-based approach that defined Vp as a function of sediment age and depth using the method of Faust (1951). These relations were defined based on sonic logs, and the model was parameterized by mapping these functions to a sediment volume that included several geologic horizons of known age and depth. In a similar fashion, Brankman (2009) developed a simple non-linear function of velocity increases with depth in the Ventura basin. Lovely et al. (2006) developed a velocity parameterization for the Salton Trough that was based on sediment and total basin depths. Basin depth was shown to reflect sediment velocities in several wells because it correlated with changing sediment facies. All of these approaches, in general, are best suited to basins where velocity data are sparse and geologic units have simple, uniform velocity gradients with depth. In contrast, Suess and Shaw (2003) and Rivero et al. (2004) used geostatistical interpolations from direct velocity measurements to parameterize sediment velocities in the Los Angeles basin and Inner California Borderland, respectively. Tens of thousands of direct velocity measurements from

boreholes and stacking velocities, as well as variance analyses were used to define vertical and horizontal velocity correlation functions. Based on these functions, kriging techniques were then applied to parameterize sediment velocities. These resulting geostatistical parameterizations generally reflect the average velocity values manifest in the rule-based models, but exhibit a greater degree of complexity in internal basin structures (Suess and Shaw, 2003).

Basin structures in the USR were assembled in a manner that was compatible with these different types of sediment velocity parameterizations, as no single, effective approach could be implemented for all of the basin structures in southern California. Geostatistical parameterizations were used in the Los Angeles (after Suess and Shaw, 2003) and Santa Maria (after Munster, 2007, and Shaw and Plesch, 2012) basins, and in the Inner California Borderland (after Rivero, 2004). Simple depth-dependent velocity descriptions were used in the Ventura (after Brankman 2009) and Salton Trough (after Lovely et al., 2006) basins. The San Bernardino basin was parameterized by a depth-dependent rule based on local well log data and seismologic studies (Stephenson et al., 2002; Anderson et al., 2004; and Graves, 2008). To blend these different local velocity parameterizations into a single USR, we used the basement surface to define the extent of different velocity parameterizations and simple smoothing techniques to ensure gradual changes between regions within the sedimentary volumes. Most of these junctures occurred at transitions from onshore to offshore basins.

**3.2 The crust and upper mantle**

The initial 3D crustal velocity model of southern California used in constructing the USR was determined by tomographic inversion based on local earthquake data (Hauksson, 2000). We used the inversion code SIMULPS (Thurber, 1993) and travel time P and S-

343 P picks from the Southern California Seismic Network to determine gridded Vp and
344 Vp/Vs models with linear interpolation between adjacent nodes. The starting model was
345 similar to the standard southern California 1D layered model (Hutton et al. 2010) with a
346 near-surface low velocity layer. First, we inverted for a 40 km horizontal and ≈4km
347 vertical spacing coarse grid-node model, followed by an interpolation to a refined grid
348 (15 km horizontal and the same vertical spacing), and repeated the inversion.
349
350 To update the model by Hauksson (2000), we replaced the velocity values at nodes
351 located within the basins with velocity values from the basin models described
352 previously. We repeated the inversion using this new starting model with basin velocity
353 values held fixed, and the same travel-time data set from Hauksson (2000). The final
354 model exhibits lower average velocities in the near-surface, consistent with the basin
355 representations, and slightly higher average velocities at depth.
356
357 Mantle structure was then modeled using teleseismic surface wave data, recorded by
358 the California Integrated Seismic Network (CISN). A two-station waveform matching
359 technique was developed for these network data (Prindle and Tanimoto, 2006) and was
360 applied to 114 large earthquakes (M>6.0) to derive phase velocity variations. Rayleigh-
361 wave phase velocity data for frequencies between 0.025 and 0.050 Hz (40 to 20s) and
362 Love-wave phase velocity data between 0.030 and 0.045 Hz (33.3 to 22.2s) were
363 retrieved by this method and used as inputs for subsequent mantle structure inversion.
364
365 For the inversion of upper mantle structure, the crustal structure, obtained from the
366 previous basin descriptions and tomographic models, was held fixed. Also, because the
367 lateral resolving wavelength of surface waves is longer than what can be achieved from
368 body-wave data, this crustal velocity structure was averaged over a block size 0.2

369 degree (lat) x 0.25 degree (lon) before surface-wave inversion. The result is a mantle
370 structure that is relatively smoother (averaged over 20-30 km) in comparison to the
371 crust. This surface wave inversion approach was used to directly infer S-wave structure
372 in the model. P-wave variations in this model were derived from surface wave data only,
373 through a relation d(ln Vp)/d(ln Vs) = 0.8, and thus may be considered less accurate
374 than the S-wave structure.
375
376 In summary, this approach, of using basin velocity descriptions as a starting point for 3D
377 tomographic inversions, helps to ensure consistency between the basin, crustal, and
378 upper mantle velocity descriptions. This model, in turn, served as the starting point for
379 3D waveform tomographic inversion to further refine the crustal velocity descriptions.
380
381 **3.3 3D Adjoint waveform tomography**
382 Computational and theoretical developments over the past 15 years (Komatitsch et al.,
383 2002) have led to an era where complex seismological models, such as the CVM, can
384 be iteratively improved though formal tomographic inversion methods (e.g., Chen et al.,
385 2007; Tape et al., 2009; Fichtner et al., 2009; Lee et al., 2014a,b). Seismic wave
386 propagation codes can be used to partition a particular model into hundreds to
387 thousands of parts, allowing for an extremely large (in terms of grid points) problem to be
388 solved by parallel computing clusters. These seismic wavefield simulations produce
389 synthetic seismograms, which are highly accurate solutions to the wave equation for the
390 input structural and earthquake models.
391
392 The tomographic inverse problem starts with the specification of a misfit function
393 measuring the difference between a set of recorded seismograms and a set of synthetic
394 seismograms computed from wavefield simulations. The accuracy of the wavefield

simulations is also exploited by the tomographic inversion. The same solver can be used to compute the gradient of the misfit function, per earthquake, with respect to each model parameter, such as the shear velocity at each grid point (Tarantola 1984; Tromp et al. 2005). The individual gradients (or “event kernels”) can be used within standard gradient-based iterative optimization algorithms (e.g., Tape et al. 2007).

The CVM with basin, crust, and upper mantle velocity descriptions was used within the large-scale iterative tomographic inversion of Tape et al. (2009, 2010). The inversion included 143 regional earthquakes (Mw 3.8–5.2), each of which was recorded by up to 160 stations on three-component seismograms filtered between 2 s and 30 s. The moment tensor and depth of each earthquake source was estimated using the initial model and also the final model using the method of Liu et al. (2004).

The final model, after 16 iterations, included large perturbations (up to 40%) from the initial 3D model. The changes were concentrated in the uppermost 20 km of the crustal model and were attributed to both compositional features (e.g. the southernmost San Joaquin basin) and to thermal features (e.g., Quaternary and Holocene volcanism in the eastern Mojave). An independent set of 91 earthquakes, not used in the inversion, was used to validate the improvements between the initial and final models. The misfit reduction from the independent set of earthquakes was essentially the same as the misfit reduction for the earthquakes used in the inversion (Tape et al. 2009). These perturbations to the starting model were included in the USR for the crust. The basin representations were left unchanged, given their high resolution and the expanded representations that occurred separately during the course of the inversion, but they could be modified in future inversions.

### 3.4 Geotechnical layer (GTL)

Shallow subsurface velocity structures, particularly shear wave speeds (Vs), have a significant influence on strong ground motions. Thus, some applications for the USR require parameterization of this near surface structure. To address this need, the USR framework includes a representation of shallow subsurface Vp, Vs, and density structure in the form of a Geotechnical Layer (GTL) that can be overlain on the underlying basin and crustal velocity descriptions (Ely et al., 2010).

The GTL is based on the widely accepted use of Vs30, or average shear wave speed down to 30 meters depth, as a method of parameterizing velocities at the model's ground surface. Vs30 is measured by logging in geotechnical boreholes and can be inferred from surface geology or topographic gradients (Wald and Allen, 2007). In our GTL, we used the geology-based Vs30 maps of Wills and Clahan (2006). Vp, and in turn density, are inferred from surface Vs using the scaling laws of Brocher (2005). We evaluated a number of depth-dependent velocity formulations with the goal of effectively representing a wide range of soil and rock velocity profile types and providing a smooth transition to the underlying crustal velocity model. We sampled velocities in the underlying model at a depth of 350 meters, which corresponds roughly with the upper limit of independent velocity measurements from well data in the underlying models and typically avoided artifacts associated with the topographic surface. The selected model includes cubic and square-root depth dependence for Vp and Vs based on Boore and Joyner's (1997) generic rock profile and the velocities in the underlying model after Ely et al. (2010). The specific formulations used in these parameterizations are described in the Supplemental Information for this article. The GTL layer is provided as an optional overlay on the underlying USR, so that it can be implemented when necessary to support ground motion, seismic hazard assessment, and other applications.

446

447 **4. Assembly of the USR**

448 The upper solid surface of the USR is marked by topographic or bathymetric elevations.
449 For bathymetry we use ETOPO-1 (Amante and Eakins 2009) and, where available,
450 measurements derived from seafloor reflectors of seismic surveys. For topography we
451 used GTOPO30 (USGS, 1996). ETOPO-1 and GTOPO30 have resolutions of about 1.8
452 km and 0.9 km, respectively.

453

454 The various components of the USR, including the topography, basin representations,
455 basement and Moho surfaces, tomographic crust and upper mantle velocity models, and
456 the GTL were assembled by parameterizing a set of voxets, or regular grids of voxels,
457 with velocity values and by appropriately resampling surfaces. These nested voxets
458 include a high-resolution grid (250 by 250 m horizontally, 100 m in depth) centered
459 around the Los Angles basin, where we had the greatest density of data. This voxet was
460 embedded in a medium resolution grid (1 by 1 km resolution) for the remainder of
461 southern California. Areas beyond the extent of the voxets are extrapolated by a 1D
462 velocity model (Dreger and Helmberger, 1990; Wald et al., 1995; Hutton et al., 2010).
463 Below 15 km, the model resolution is 1 km vertically and 10 km horizontally.

464

465 Most of the data used to define the velocity structure within the sedimentary basins
466 sample Vp. Vs and rock density ($\rho$) are defined for sediments in the model using the
467 empirical relationship of Brocher (2005), which are based on well logs that independently
468 constrained Vp, Vs, and density. The tomographic crust and upper mantle models define
469 both Vp and Vs, and the GTL specifies Vp and Vs values as described in the
470 Supplemental Information. Thus, Vs values for these model components were used
471 directly to parameterize the USR.

The USR is accessed through the SCEC website, where users download the voxets and use a query tool to parameterize arbitrary points (x, y, and z) with Vp, Vs, $\rho$. The code delivers these values, along with the properties we described, for the closest grid point in the model, along with the precise location of that grid point. The basement surface and Moho are provided as separate structural elements (tsurfs) along with the voxets. In addition, every grid point within the voxets contains properties that describe the region of the model that they represent (sediment, crust, upper mantle). Properties also specify the vertical distance to the basement and Moho horizons, which is useful information for developing computational meshes or grids. The USR is provided through the SCEC website as a series of CFM and CVM model components. CFM version 5.0 and CVM-H 15.1.0 are used for this manuscript. For a discussion of model resolution and uncertainty, the reader is referred to the Supplemental Information accompanying this article.

## 5. Description

The primary velocity structures in the upper crust of southern California are the deep sedimentary basins. Average velocity functions for sediments within these basins all show general trends of increasing velocity with depth (Fig. 6A). Notably, the average velocity profiles for the Los Angeles, Ventura, and Santa Barbara basins are similar, reflecting that these basins contain comparable Neogene to recent stratigraphic sequences. The Inner California Borderland exhibits a similar velocity gradient to these basins, with the exception of a shallow (≈ 500 m) velocity inversion that is associated with a Tertiary volcanic section inter-bedded with sediments (Crouch and Suppe, 1990; Bohannon and Geist,1998; Rivero, 2004). The Santa Maria and San Bernardino basins also show broadly similar velocity gradients, yet typically exhibit faster velocities at

shallow depths. This results from thinner Pliocene and younger sedimentary strata in these basins. In contrast, the Salton Trough basin shows very slow near surface velocities, but also the steepest velocity gradient of any basin from about 200 to 3000m depths. This rapid increase in velocities likely reflects the high geothermal gradient in the area, which lithifies and metamorphoses the sediments thereby increasing their wavespeeds and densities

Lateral variations in velocities modeled within the basins reflect both the amount of the data that were used to parameterize them as well as sedimentological and tectonic controls. The Los Angeles, Ventura, and Santa Maria basins have the greatest sediment thicknesses (up to ≈ 10, 12, and 5 km, respectively), and the highest density of direct velocity data coverage from well and seismic reflection data (Suess and Shaw, 2004; Munster, 2007; Brankman, 2009). These basins generally exhibit the largest lateral contrasts in velocities (from 1.5 to 4.5 km/s) at shallow depths (< 2 km), due to situations where faults laterally juxtapose faster, older sedimentary rocks with slower, younger sediments. Below 2 km, sediment velocities generally exhibit smaller, but nonetheless significant lateral variations. In the Los Angeles basin, for example, modeled sediment velocities vary laterally by about 1 km/s from 2 to 7 km, representing a variance of about 20 to 30% from the average velocity values (Fig. 6B). This pattern reflects compaction and diagenesis of the different types of clastic sedimentary sections that comprise the basin (Suess and Shaw, 2004). Moreover, these strata have also been folded and uplifted by faulting, producing lateral juxtapositions of different lithologic units. The most significant lateral variations in velocity occur across major faults, including both thrust and strike-slip systems. In the Los Angeles basin, the Newport-Inglewood, Palos Verdes, Puente Hills, and Whittier faults all produce abrupt, local velocity contrasts within the sedimentary strata. Moreover, these as well as other structures, including the Santa

Monica fault, locally juxtapose crystalline basement adjacent to, or above, the sedimentary strata (Fig. 5). These fault boundaries can produce local increases in velocity (Vp) of more than 350% moving from unconsolidated sediments to basement rocks. The Ventura basin also exhibits such abrupt velocity gradients, mainly along the San Cayetano, Ventura, Pitas Point, and Oak Ridge faults. Similar lateral velocity variations in the Santa Maria basin result from a series of east-west trending folds that are underlain by blind-thrust faults (Munster, 2007; Shaw and Plesch, 2012).

These basin descriptions, when combined with the tomographic models and overlain by the GTL, provide a comprehensive description of the crust and upper mantle structure in southern California (Figs. 7 and 8). Beginning at the shallowest depths (0 to 300m), the changes from near-surface to deeper sediment velocities are significant (≈ 800 to 2400 m/s). However, the transition is smooth given that the GTL used underlying velocity values in its parameterization (Fig. 7) [see electronic supplement]. The near surface velocities in the GTL vary across the model as a function of rock types, with the slowest velocities in the sedimentary basins, intermediate velocities in ranges comprised of sedimentary rock, and the fastest velocities in regions that expose crystalline rocks (Fig. 7). The sedimentary basins are characterized by increasing velocity with depth, yet include internal velocity variations due to changes in lithology and the presence of faults. At the bottom of the sedimentary basins, velocities generally change abruptly across the top basement horizon (Figs. 8 and 9). These contrasts are greatest (≈ from 2000 to 5,500 m/s) in shallow parts of the basins, where sediments are poorly lithified. In the deepest part of basins, velocity changes across the sediment-basement interface are substantially less (≈ from 4,500 to 5,500 m/s). This results from the compaction of sedimentary units at depth, yielding faster velocities that approach those of the underlying basement rocks.

The underlying crust and mantle structure exhibit general trends that reflect the major tectonic elements in southern California (Fig. 8). In the upper 15 kilometers of the crust, low velocity roots are present beneath most of the sedimentary basins. This pattern may result, in part, from a smearing of the low velocity basins to depth in the tomographic models. However, it may also reflect crustal thinning related to the Neogene rifting and formation of the basins. A similar low-velocity region underlies the San Gabriel Mountains and Coast Ranges, which contain deformed early Tertiary sedimentary and metasedimentary sections that were not explicitly represented in the model. In contrast, the Peninsular Ranges are underlain by a fast velocity region (Fig. 9A). This likely reflects the deep crystalline roots of these Ranges, which correspond with one of the thickest areas of continental crust in southern California (Fig. 3).

The USR is compared with the velocity model of Lee et al. (2014b,a) at shallow depths in Figure 8. Lee et al. (2014b,a) applied full-3D tomography using a combination of the scattering-integral method and the adjoint-wavefield method to iteratively improve a 3-D starting model of the southern California based on Magistrale et al., (2000). These authors provided a formal comparison of their model to a version of the crustal velocity description incorporated in the USR to which the readers are referred. In Figure 8 we highlight the difference in model representations at shallow crustal levels where basin and fault structures have the greatest influence on velocity structure. Both models show low velocity sediments within the Los Angles and other basins. However, the USR exhibits larger basins that extend offshore and include more complex internal velocity structures. These internal velocity structures result from the larger well and seismic reflection datasets that were used as constraints in the USR, and the incorporation of faults that directly influence basin geometries.

## 6. Applications to earthquake simulations

A fundamental use for the USR is to provide the most accurate information available (faults and velocity structure) for earthquake simulations. These simulations, in turn, can be used to obtain better estimates of earthquake source models (e.g., Liu et al., 2004). The CVM has been tested with earthquake simulations (Komatitsh et al., 2004; Lovely et al. 2007; Tape et al. 2009; Graves and Aagaard, 2011) and with ambient noise cross correlations (Ma et al. 2008). A second purpose of the earthquake simulations is to iteratively improve the CVM.

We demonstrate the importance of 3D structure on realistic earthquake simulations in Figures 9 and 10. We consider a Mw 7.9 scenario thrust earthquake that is approximately aligned with the Ventura-Pitas Point fault system (Hubbard et al., 2014). The earthquake rupture model (Figure 9a) is the 2008 Wenchuan, China, earthquake, which is one of the largest continental thrust faults recorded in the past decade (Shao et al., 2010). The kinematic source model is derived from seismic and geodetic observations using the method of Ji et al. (2002).

The earthquake simulation is performed using SPECFEM3D software (Komatitsch et al., 2004; Peter et al., 2011), which uses a spectral element method for representing wave propagation on unstructured hexahedral finite element meshes. The wavefield is computed throughout the volume, and synthetic seismograms are saved at designated points. From each synthetic seismogram, the peak velocity is saved and plotted in Figure 9. Comparison of Figures 9b and 9c, which show the computer peak velocities from the regional 1-D model and the USR, respectively, demonstrate the well-known

602 effect of the amplification of seismic waves from basin structures (e.g., Komatitsch et al.,
603 2004, Graves, 2008).
604
605 The wavefield simulations contain far more information than is represented in the peak
606 ground velocity maps. Snapshots of the simulations (Figure 10) show the influence of
607 the 3D basin structures (and topography) on the seismic wavefield. The simulation in the
608 1D model reveals a strong source pulse directed to the southeast. This pulse is much
609 weaker in the 3D model, where much of the energy is trapped within the basin
610 structures. These results illustrate the importance of using realistic models of velocity
611 and fault structure such as the USR in forecasting the amplitude and duration of
612 hazardous ground shaking that will result from large earthquakes.
613
614 **7. Conclusion**
615 We present a methodology for developing precise and internally consistent descriptions
616 of Earth structure that span the range of wavespeed from low velocity sediments in the
617 shallow subsurface to upper mantle structure. This involves the careful integration of
618 many datasets, including borehole observations, seismic reflection and refraction
619 surveys, and earthquake body and surface wave data. The workflow that we have
620 developed for constructing the USR, involving development of basin descriptions, crust
621 and upper mantle tomography, and 3D adjoint waveform tomography, ensures the
622 internal consistency of the model components and promotes the accuracy of the
623 integrative model. We illustrate this implementation through the development of a USR
624 for southern California, which describes heterogeneous wavespeed structure in the crust
625 that formed over a long and complex tectonic history. Finally, we illustrate the value of
626 compatible fault and velocity representations in the USR through a simulation of a
627 hypothetical M 7.9 earthquake on thrust faults in the Western Transverse Ranges. This

simulation highlights the influence of fault and basin structure in controlling the distribution and duration of hazardous ground shaking that may result from future earthquakes.

**Figure captions**

1) Perspective view of components of the Unified Structural Representation (USR). A) Topography and bathymetry; B) top basement surface; C) Community Fault Model (CFM) (Plesch et al., 2007); and D) USR showing Vp. SAF is the San Andreas fault. Topographic and bathymetric surfaces are derived from USGS 3″ digital elevation model data and a National Oceanic and Atmospheric Administration 30″ grid (TerrainBase).

2) Map of southern California showing major basins, mountain ranges, and faults noted in the text. LA is Los Angles basin; V is Ventura basin, IB is Inner Borderland; SM is Santa Maria basin; SB is Santa Barbara basin; B is the San Bernardino basin. SAF is the San Andreas fault; ECSZ is the Eastern California Shear Zone; G is the Garlock fault; SJF is the San Jacinto fault. Section traces are for profiles plotted in Figure 7. Arrows signify endpoints of sections X and Y that are located outside the map.

3) Moho depth surface in the CVM, from Tape et al. (2012). The colored circles indicate the locations of measured points used in estimating the surface; most are from receiver function studies (e.g., Gilbert et al., 2012) or from wide-angle refraction studies.

4) Sample of data used to define the basement horizon and velocity structure within sedimentary basins. (left) Migrated seismic reflection profile in depth from the Inner California Borderland showing prominent top basement horizon. Log of Vp derived from sonic logs in a well located northeast of the seismic section, and shown with the same vertical scale. For Vp, both the raw data (black) and a running 25 m average (red) are shown. Note the prominent velocity increase that occurs at the bottom of the log where the well penetrates basement.

5) Perspective view looking north of the top basement surface in depth with faults from the Community Fault Model (CFM) (Plesch et al., 2007). Note that steeply dipping strike- and oblique-slip faults, such as the Newport-Inglewood and Whittier systems, form steep boundaries to the basin. Moderately dipping thrust faults, such as the Santa Monica and Puente Hills thrust, locally duplicate the sediment-basement horizon. The Anaheim fault is considered to be an inactive structure, and thus is not represented in the CFM. However, the fault is included in the USR because it influences the basin shape. PHT is the Puente Hills thrust fault. Filled teeth represent surface emergent faults; open teeth represent blind faults.

6) Plots of velocity (Vp) in sedimentary basins represented in the USR. (left) Average velocity functions for each basin. (right) Average velocity function for the Los Angeles basin superimposed on the distribution of velocity values for the basin included in the model.

7A) Perspective view of the northern part of the USR, showing an enlarged transect across the Los Angeles basin. An enlarged view of the shallow velocity structure in the basin shows the Geotechnical Layer (GTL), as described in the text. B) Cross sections showing Vp across the USR. Section traces are shown in Figure 2. LA is Los Angeles basin; SB is Santa Barbara basin; IB is Inner Borderland; ST is Salton Trough basin.

8) Depth slices at – 1000 m elevation comparing Vp from the USR (left) and CVM-S 4.26 (Lee et al., 2014a,b) (right). LA is Los Angeles basin; IB is Inner Borderland; SB is Santa Barbara basin; SF is San Fernando basin; SM is Santa Maria basin; ST is Salton Trough basin; V is Ventura basin.

9) The influence of 3D structure on the seismic wavefield, Part I. (a) Mw 7.9 finite-source model (Ji et al., 2002) for the Wenchuan, China, earthquake (Shao et al., 2010). The model is discretized with 61,970 subsources; the color denotes the moment associated with each subsource. (b) Peak ground velocity at a selected number of points within the simulation using a 1D layered structural model (Dreger and Helmberger, 1990; Wald et al., 1995). (c) Peak ground velocity using USR (CVM-H 15.1.0). Ground velocities are much larger in the regions containing deep sedimentary basins, which trap and amplify seismic waves.

10) The influence of 3D structure on the seismic wavefield, Part II. The left column shows snapshots of a seismic wavefield simulation performed for the earthquake source model in Figure 9a and using a 1D structural model. The right column shows the same simulation, but instead using the 3D USR structural model (CVM-H 15.1.0). The colors of the wavefield represent the vertical component of velocity. The background gray is the uppermost surface of the finite-element mesh in the simulation; hence, the topography is only visible in the right column. Note the strong, long-lasting shaking within the basin structures of USR.

## References


Aagaard, B. T., J. F. Hall, and T. H. Heaton, 2001, Characterization of near-source ground motions with earthquake simulations, Earthquake Spectra 17, no. 2, 177–207.

Abrahamson, N. A., and W. J. Silva, 1997, Empirical Response Spectral Attenuation Relations for Shallow Crustal Earthquakes, *Seismological Research Letters*, *68*(1), 94-127.

Abrahamson, N. A., and W. J. Silva, 2008, Summary of the Abrahamson & Silva NGA Ground-Motion Relations, *Earthquake Spectra*, *24*(1), 67-97.

Allen, C. R., 1981, The modern San Andreas fault, in The Geotectonic Development of California, edited by W. G. Ernst, Prentice-Hall, Englewood Cliffs, N.J., pp. 511-534.

Allen, C. R., 1957, San Andreas fault zone in San Gorgonio Pass, southern California, Geol. Sac. Am. Bull., 68, 315-350.

Amante, C., and B. W. Eakins, 2008, ETOPO1 1 Arc-Minute Global Relief Model: Procedures, Data Sources and Analysis, National Geophysical Data Center, NESDIS, NOAA, U.S. Dept. Commerce, Boulder, Colo., USA.

Anderson, M., J. Matti, and R. Jachens, 2004, Structural model of the San Bernardino basin, California, from analysis of gravity, aeromagnetic, and seismicity data, J. Geophys. Res., 109, B04404, doi:10.1029/2003JB002544.

Astiz, L., and C. R. Allen, 1983, Seismicity of the Garlock fault, California, Bull Seismo. Soc. Am., 73, 1721-1734.

Atwater, T, 1970, Implications of plate tectonics for the Cenozoic tectonic evolution of western North America, Geol. Soc. Am. Bull., 81, 3513-3536.

Bielak, J., J. Xu, and O. Ghattas, 1999, Earthquake ground motion and structural response in alluvial valleys, Journal of Geotechnical Geoenvironmental Engineering 125, 413–423.

Bielak, J., R. Graves, K. Olsen, R. Taborda, L. Ramirez-Guzman, S. Day, G. Ely, D. Roten, T. Jordan, P. Maechling, J. Urbanic, Y. Cui , and G. Juve, 2010, The ShakeOut earthquake scenario: verification of three simulation sets, Geophys. J. Int., 180, 375-404.

Bird, P., and R.W. Rosenstock,1984, Kinematics of present crust and mantle flow in southern California Geol.Soc.Am.Bull., 95, 946-957

Bohannon, R. and Geist, E., 1998, Upper crustal structure and Neogene tectonic development of the California continental borderland: Geological Society of America Bulletin, v. 110, p. 779-800.

Boore, D. M., and G. M. Atkinson, 2008, Ground-motion prediction equations for the average horizontal component of PGA, PGV, and 5%-Damped PSA at spectral periods between 0.01s and 10.0s, *Earthquake Spectra*, *24*(1), 99-138.

Bonamassa, O., and J. E. Vidale, 1991, Directional site resonances observed from aftershocks of the 18 October 1989 Loma Prieta earthquake, BSSA, v.81, p. 1945-1957.

Bouchon, M., and J. S. Barker, 1996, Seismic response of a hill: the example of Tarzana, California, BSSA, v.86, p.66-72.

Brankman, C., 2009, Three-Dimensional Structure of the Western Los Angeles and Ventura Basins, and Implications for Regional Earthquake Hazards, Ph.D. dissertation, Harvard University, Cambridge, MA, USA, 133 p.

Brocher, T.M., 2005, A regional view of urban sedimentary basins in Northern California based on oil industry compressional-wave velocity and density logs, Bulletin of the Seismological Society of America, vol.95, no.6, pp.2093-2114.

Burchfiel, B.C., K- V. Hodges, and L. H. Royden, 1987, Geology of Panamint Valley-Saline Valley pull-apart system, California: Palinspastic evidence for low-angle geometry of a Neogene range bounding fault, J. Geophys Res. es.,9 2, 10,422-10,426.

Chen, P., T. H. Jordan, and L. Zhao, 2007, Full three-dimensional waveform tomography: a comparison between the scattering-integral and adjoint-wavefield methods, Geophys. J. Int., 170,175-181, doi: 10.1111/j.1365-246x.2007.03429.x.

Cowan, D. S., & Bruhn, R. L., 1992, Late Jurassic to early late Cretaceous geology of the U.S. cordillera, in Burchfiel B. C., Lipman P. W. and Zoback M. L. (Eds.), The Cordilleran Orogen; conterminous U.S. United States, Geol. Soc. Am., p. 169-203.

Crouch, J. K. and Suppe, J., 1993, Late Cenozoic tectonic evolution of the Los Angeles basin and inner California borderland: A model for core complex-like crustal extension: Geological Society of America Bulletin, v. 105, p. 1415-1434.

Curray, J. R. and Moore, D. G., 1984, Geologic History of the Mouth of the Gulf of California, in Crouch, J. K., and Bachman, S. B., eds., Tectonics and Sedimentation along the California Margin: Pacific Section S.E.P.M., v. 38, p. 17-35.

Dreger, D. S., and D. V. Helmberger, 1990, Broadband modeling of local earthquakes, Bull. Seis. Soc. Am., 80(5), 1162–1179.

DeMets, C. Gordon, R. G., Stein, S., and Argus, D. F., 1987, A revised estimate of Pacific-North America motion and implications for western North America plate boundary zone tectonics: Geophysical Research Letters, v. 14, no. 9, p. 911- 914.

Dibblee, T. W., Jr., 1950-2005, Geologic map series, California [Map]. 1:24,000. Santa Barbara, CA:Thomas W. Dibblee, Jr. Geol. Found.

Dickinson, W.R., 1981, Plate tectonics and the continental margin of California, in Ernst, W.G., ed., The Geotectonic Development of California (Rubey Volume I): Englewood Cliffs, New Jersey, Prentice-Hall, p. 1–28.

Dokka, R. K., and C. Travis, 1990, Role of the eastern California Shear Zone in accommodating Pacific-North American plate motion, Geophysical Research Letters, 17/9, 1323-1326.

Ely, G., T. H. Jordan, P. Small, P. J. Maechling, 2010, A Vs30-derived Near-surface Seismic Velocity Model Abstract S51A-1907, presented at 2010 Fall Meeting, AGU, San Francisco, Calif., 13-17 Dec.

Ernst, W.G., 1970, Tectonic contact between the Franciscan mélange and the Great Valley sequence—Crustal expression of a late Mesozoic Benioff zone: Journal of Geophysical Research, v. 75, p. 886–902, doi: 10.1029/ JB075i005p00886.

Faust, L. Y., 1951, Seismic velocity as a function of depth and geologic time, Geophysics 16, 192–206.

812 Field, E. H., 2000, A modified ground-motion attenuation relationship for southern California that
813 accounts for detailed site classification and a basin-depth effect, *Bulletin of the Seismological*
814 *Society of America*, *90*(6b), s209-s221.
815
816 Fichtner, A., B. L. N. Kennett, H. Igel, and H.-P. Bunge (2009), Full seismic waveform
817 tomography for upper-mantle structure in the Australasian region using adjoint methods,
818 Geophys. J. Int., 179, 1703–1725.
819
820 Frankel, A., and J. Vidale, 1992, A three-dimensional simulation of seismic waves in the Santa
821 Clara valley, California, from the Loma Prieta aftershock, Bulletin of the Seismological Society of
822 America 82, 2045–2074.
823
824 Fuis, G., and W. Kohler, 1984, Crustal structure and tectonics of the Imperial Valley Region,
825 California, in Rigsby, C.A., The Imperial Basin-Tectonics, Sedimentations, and Thermal aspects:
826 Pacific Section SEPM, p1-13.
827
828 Graves, R., 2008, The seismic response of the San Bernardino basin region during the 2001 Big
829 Bear Lake earthquake, Bulletin of the Seismological Society of America, Vol. 98, No. 1, pp. 241–
830 252, doi: 10.1785/0120070013.
831
832 Graves, R. W., and B. T. Aagaard, 2011, Testing Long-Period Ground-Motion Simulations of
833 Scenario Earthquakes Using the Mw 7.2 El Mayor-Cucapah Mainshock: Evaluation of Finite-Fault
834 Rupture Characterization and 3D Seismic Velocity Models*, Bull Seism. Soc. Am.*, **101**, doi:
835 10.1785/012100233.
836
837 Graves, R.W., Pitarka, A., Somerville, P. G., 1998, Ground-motion amplification in the Santa
838 Monica area; effects of shallow basin-edge structure, Bulletin of the Seismological Society of
839 America, vol.88, no.5, pp.1224-1242.
840
841 Graves, R., T.H. Jordan, S. Callaghan, E. Deelman, E. Field, G. Juve, C. Kesselman, P.
842 Maechling, G. Mehta, K. Milner, D. Okaya, P. Small, and K. Vahi, 2011, CyberShake: A Physics-
843 Based Seismic Hazard Model for Southern California, Pure Appl. Geophys. 168, 367–381 Ó 2010
844 Springer Basel AG DOI 10.1007/s00024-010-0161-6.
845
846 Hamilton, W., 1969, Mesozoic California and the under- flow of Pacific mantle: Geological Society
847 of America Bulletin, v. 80, p. 2409–2430, doi: 10.1130/ 0016-
848 7606(1969)80[2409:MCATUO]2.0.CO;2.
849
850 Hauksson, E., 2000, Crustal structure and seismicity distributions adjacent to the Pacific and
851 north America plate boundary in southern California, *J. Geophys. Res.*, *105*, 13,875-13,903.
852
853 Hill, M. L., and T. W. Dibblee, Jr., 1953, San Andreas, Garlock, and Big Pine faults, California: a
854 study of the character, history, and tectonic significance of their displacements, Geol. Soc. Am.
855 Bull. 64, 443–458.
856
857 Hornafius, J. Scott; Luyendyk, Bruce P.; Terres, R. R.; Kamerling, M. J., 1986, Timing and extent
858 of Neogene tectonic rotation in the western Transverse Ranges, California, Geological Society of
859 America Bulletin, vol.97, no.12, pp.1476-1487.
860
861 Hubbard, J., J. H. Shaw, J. Dolan, T. L. Pratt, L. McAuliffe, and T. K. Rockwell, 2014, Structure
862 and seismic hazard of the Ventura Avenue anticline and Ventura fault, California: Prospect for
863 large, multisegment ruptures in the Western Transverse Ranges, BSSA,
864 doi:10.1785/0120130125.
865
866 Huftile, G. J., and R. S. Yeats, 1995, Convergence rates across a displacement transfer zone in
867 the western Transverse Ranges, Ventura Basin, California, J. Geophys. Res. 100 (B2), 2043–

2067.

Humphreys, E. D., and Hager, B. D., 1990, A kinematic model for the Late Cenozoic development of southern California crust and upper mantle: Journal of Geophysical Research, v. 95, no. B12, p. 19,747-19,762.

Hutton, L. K., J. Woessner, and E. Hauksson, Seventy-seven years (1932 – 2009) of earthquake monitoring in southern California, 2010, *Bull. Seismol. Soc. Am*, v. 100; no. 2; p. 423-446; DOI: 10.1785/0120090130.

Jennings, C.W., Strand, R.G., and Rogers, T.H., 1977, Geologic map of California: California Division of Mines and Geology, scale 1:750,000.

Ji, C., D. J. Wald, and D. V. Helmberger, 2002, Source description of the 1999 Hector Mine, California, earthquake, Part I: Wavelet domain inversion theory and resolution analysis, Bull. Seis. Soc. Am., 92(4), 1192-1207.

Kamerling, M. J., & Luyendyk, B. P. (1985). Paleomagnetism and neogene tectonics of the Northern Channel Islands, California. *Journal of Geophysical Research, 90*, 12-12,502. doi:http://dx.doi.org/10.1029/JB090iB14p12485

Komatitsch, D., J. Ritsema, and J. Tromp, 2002, The spectral-element method, Beowulf computing, and global seismology, Science, v. 298, 1737-1742.

Komatitsch, D., & J. Tromp, 1999, Introduction to the spectral element method for three-dimensional seismic wave propagation. Geophys. J. Int., 139, 806-822;

Komatitsch, D., Q. Liu, J. Tromp, P. Suess, C. Stidham, and J. H. Shaw, 2004, Simulations of Ground Motion in the Los Angeles Basin Based upon the Spectral Element Method, Bulletin of the Seismological Society of America 94, 187-206.

Lee, E.-J., P. Chen, and T. H. Jordan (2014a), Testing waveform predictions of 3D velocity models against two recent Los Angeles earthquakes, Seis. Res. Lett., 85(6), 1275–1284.

Lee, E.-J., P. Chen, T. H. Jordan, P. B. Maechling, M. A. M. Denolle, and G. C. Beroza (2014b), Full-3D tomography for crustal structure in Southern California based on the scattering integral and the adjoint-wavefield methods , J. Geophys. Res. Solid Earth, 119, 6421–6451, doi:10.1002/2014JB011346.

Legg, M., and C. Nicholson, 1993, Geologic structure and tectonic evolution of the San Diego Trough and vicinity, California continental borderland: AAPG Bulletin, v. 77, p. 705.

Lin, G., P. M. Shearer, and E. Hauksson, 2007, Applying a three-dimensional velocity model, waveform cross correlation, and cluster analysis to locate southern California seismicity from 1981 to 2005, *J. Geophys. Res.*, **v.112**, n.B12, 14 pp, B12309, doi:10.1029/2007JB004986.

Liu, Q., J. Polet, D. Komatitsch, and J. Tromp, 2004, Spectral-element moment tensor inversions for earthquakes in southern California, Bull. Seis. Soc. Am., 94(5), 1748-1761.

Lovely, P., J. H. Shaw, Q. Liu, and J. Tromp, 2006, A Structural VP Model of the Salton Trough, California, and Its Implications for Seismic Hazard, Bulletin of the Seismological Society of America, Vol. 96, No. 5, pp. 1882–1896.

Luyendyk, Bruce P; Kamerling, Marc J; Terres, Richard Ralph; Hornafius, John Scott, 1985, Simple shear of Southern California during Neogene time suggested by paleomagnetic declinations, Journal of Geophysical Research, vol. 90, no. B14, pp.12,454-12,466.

Ma, S., G. A. Prieto, and G. C. Beroza, 2008, Testing community velocity models for southern California using the ambient seismic field, Bull. Seis. Soc. Am., 98(6), 2694-2714.

Magistrale, H., S. Day, R. W. Clayton, and R. Graves, 2000, The SCEC southern California reference three-dimensional seismic velocity model Version 2, Bull. Seism. Soc. Am. 90, S65–S76.

McCulloh, T. H. , 1960, Gravity variations and the geology of the Los Angeles basin of California, U.S. Geol. Surv. Profess. Pap. 400-B, 320–325.

McGill, S., and K. Sieh, 1993, Holocene Slip Rate of the Central Garlock Fault in Southeastern Searles Valley, California, J. Geophys. Res., 98(B8), 14,217–14,231, doi:10.1029/93JB00442.

Meade, B. J. and B. H. Hager, 2005, Block models of crustal motion in southern California constrained by GPS measurements, Journal of Geophysical Research, 110, B03403, doi:10.1029/2004JB003209.

Minster, J. B. and Jordan, T. H., 1978, Present-day plate motions: Journal of Geophysical Research 83, p. 5331-5354.

Minster, J. B., and T. H. Jordan, 1987, Vector constraints on western U.S. deformation from space geodesy, neotectonics, and plate motions, J . Geophy. Res., 9, 4798-4804.

Minster, J., Olsen, K B. Moore, R., Day, S., Maechling, P., Jordan, T., Faerman, M., Cui, Y., Ely, G., Hu, Y., Shkoller, B., Marcinkovich, C., Bielak, J., Okaya, D., Archuleta, R., Wilkins- Diehr, N., Cutchin, S., Chourasia, A., Kremenek, G., Jagatheesan, A., Brieger, L., Majundar, A., Chukkapalli, G., Xin, Q., Banister, B., Thorp, D., Kovatch, P., Diegel, L., Sherwin, T., Jordan, C., Thiebaux, M., Lopez, J., 2004, The SCEC TeraShake Earthquake Simulation Eos Trans. AGU, 85(47), Fall Meet. Suppl., Abstract SF31B-05.

Munster, J., 2007, Velocity Model of the Santa Maria Basin, CA, and its implications for seismic hazard assessment, Harvard University undergraduate thesis, 80 p.

Namson, J., and T. Davis, 1988, Structural transect of the western Transverse Ranges, California: Implications for lithospheric kinematics and seismic risk evaluation, Geology 16, 675–679.

Namson, J. and Davis, T. L., 1990, Late Cenozoic Fold-And-Thrust Belt Of The Southern Coast Ranges And Santa-Maria Basin, California, AAPG Bulletin-American Association of Petroleum Geologists 74(4): 467-492.

Nicholson, C., Sorlien, C.C., Atwater, T., Crowell, J.C., and Luyendyk, B.P., 1994, Microplate capture, rotation of the Transverse Ranges, and initiation of the San Andreas transform as a low-angle fault system, Geology, V22, p. 491-495.

Olsen, K. B., R. J. Archuleta & J. R. Matarese, 1995, Three-dimensional simulation of a magnitude 7.75 earthquake on the San Andreas fault, Science, 270, 1628-1632;

Olsen, K.B. (2000). Site Amplification in the Los Angeles Basin from 3D Modeling of Ground Motion, *Bull. Seis. Soc. Am.* **90**, S77-S94.

Peter, D., D. Komatitsch, Y. Luo, R. Martin, N. Le Goff, E. Casarotti, P. Le Loher, F. Magnoni, Q.

Liu, C. Blitz, T. Nissen-Meyer, P. Basini, and J. Tromp, 2011, Forward and adjoint simulations of seismic wave propagation on fully unstructured hexahedral meshes, Geophys. J. Int., 186, 721–739.

Plesch, A., and J. H. Shaw, C. Benson, W.A. Bryant, S. Carena, M. Cooke, J. F. Dolan, G. Fuis, E. Gath, L. Grant, E. Hauksson, T. H. Jordan, M. Kamerling, M. Legg, S. Lindvall, H. Magistrale, C. Nicholson, N. Niemi, M. E. Oskin, S. Perry, G. Planansky, T. Rockwell, P. Shearer, C. Sorlien, M. P. Suess, J. Suppe, J. Treiman, and R. Yeats, 2007, Community Fault Model (CFM) for Southern California, *Bulletin of the Seismological Society of America*, Vol. 97, No. 6, pp. 1793–1802.

Reed, R. D., and Hollister, J. S., 1936, Structural evolution of southern California: Tulsa, Oklahoma, American Association of Petroleum Geologists, 157 p.

Rivero, C., 2004, Origin of Active Blind–Thrust Faults in the southern Inner California Borderland, Ph.D. dissertation, Harvard University, Cambridge, MA, USA, 176 p.

Rivero, Carlos, and John H. Shaw, 2011, Active folding and blind thrust faulting induced by basin inversion processes, inner California borderlands, in K. McClay, J. Shaw, and J. Suppe, eds., Thrust fault-related folding: AAPG Memoir 94, p. 187 – 214.

Rockwell, T., and A. G. Sylvester, 1979, Neotectonics of the Salton Trough, in Tectonics of the Juncture between the San Andreas Fault System and the Salton Trough, Southeastern CA: A Guidebook, J. C. Crowell and A. G. Sylvester (Editors), Department of Geological Sciences, University of California, Santa Barbara, 41–52.

Savage, J. C., M. Lisowski, and W. H. Prescott, 1990, An apparent shear zone trending north-northwest across the Mojave Desert into Owens Valley, eastern California, Geophys. Res. Lett., 17(12), 2113

Shao, G., Ji, C., Lu, Z., Hudnut, K., Zhang, W., Wang, Q., 2010, Slip History of the 2008 Mw 7.9 Wenchuan Earthquake Constrained by Jointly Inverting Seismic and Geodetic Observations, Abstract S52B-04 presented at 2010 Fall Meeting, AGU, San Francisco, Calif., 13-17 Dec.

Shaw, J.H., and A. Plesch, 2012, 3D Structural Velocity Model of the Santa Maria Basin, CA, for Improved Strong Ground Motion Prediction, National Earthquake Hazards Reduction Program (NEHRP), Final Technical Report, Grant G12AP20020.

Shaw, J.H. and J. Suppe, 1994, Active faulting and growth folding in the eastern Santa Barbara Channel, California, *Geological Society of America Bulletin*, 106/5, 607-626.

Shaw, J.H., and J. Suppe, 1996, Earthquake hazards of active blind-thrust faults under the central Los Angeles basin, California, *Journal of Geophysical Research*, 101/B4, 8623-8642.

Shearer, P., E. Hauksson, and G. Lin, Southern California hypocenter relocation with waveform cross correlation: Part 2. Results using source-specific station terms and cluster analysis, *Bull. Seismol. Soc. Am.*, **95**, 904-915, doi: 10.1785/0120040168, 2005.

Smith, G.I., 1975, Holocene movement on the Garlock fault, U.S. Geol. Surv. Prof. Pap., 975, p. 202.

Smith,G .I.,1962, Large lateral displacement on the Garlock fault, California, as measured from offset dike swarms, Bull. Am. Assoc. Petrol. Geol, 4 6, 86-104.

Smith, G .I., and I. B. Ketner, 1970, Lateral displacement on the Garlock fault, southeastern California, suggested by offsets sections of similar metasedimentary rocks, U .S. Geol, Surv.Prof.

Pap. 700-D, D1-D9.

Stephenson, W. J., J. K. Odum, R. A. Williams, and M. L. Anderson, 2002, Delineation of Faulting and Basin Geometry along a Seismic Reflection Transect in Urbanized San Bernardino Valley, California, Bulletin of the Seismological Society of America, Vol. 92, No. 6, pp. 2504–2520.

Suess, P., and J. H. Shaw, 2003, P wave seismic velocity structure derived from sonic logs and industry reflection data in the Los Angeles basin, California, J. Geophys. Res. 108, no B3, doi 10.1029/2001JB001628.

Tape, C., Q. Liu, and J. Tromp, 2007, Finite-frequency tomography using adjoint methods — Methodology and examples using membrane surface waves, Geophys. J. Int., 168, 1105–1129.

Tape, C., Q. Liu, A. Maggi, and J. Tromp, 2009, Adjoint tomography of the southern California crust, Science, v. 325, p. 988-992.

Tape, C., Q. Liu, A. Maggi, and J. Tromp, 2010, Seismic tomography of the southern California crust based on spectral-element and adjoint methods, Geophys. J. Int., 180, 433–462.

Tape, C., A. Plesch, J. H. Shaw, and H. Gilbert, 2012, Estimating a continuous Moho surface for the California Unified Velocity Model, *Seismological Research Letters*, Volume 83, Number 4, 728-735.

Tarantola, A., 1984, Inversion of seismic reflection data in the acoustic approximation, Geophysics, 49, 1259-1266.

Thurber, C. H., 1993, Local earthquake tomography: velocities and Vp/Vs-theory, in Seismic Tomogrphy: Theory and Practice, edited by H. M. Iyer and K. Hirahara, pp. 563– 583, Chapman and Hall, London.

Tromp, J., C. Tape, and Q. Liu, 2005, Seismic tomography, adjoint methods, time reversal and banana-doughnut kernels, Geophys. J. Int., 160, 195-216;

Tsutsumi, H., R. S. Yeates, and G. J. Huftile, 2001, Late Cenozoic tectonics of the northern Los Angeles fault system, California, Geol. Soc. Am. Bull., 113, 454– 468.

US Geological Survey. 1996. GOTPO30 Global Digital Elevation Model. Sioux Falls, South Dakota, EROS Data Center.

Wald, D. J., and T. I. Allen, 2007, Topographic slope as a proxy for seismic site conditions and amplification, Bull. Seism. Soc. Am., 97 (5), 1379-1395, doi:10.1785/0120060267.

Wald, L. A., L. K. Hutton, and D. D. Given, 1995, The Southern California Network Bulletin: 1990–1993 summary, Seis. Res. Lett., 66(1), 9–19.

Wright, T. L., 1991, Structural geology and tectonic evolution of the Los Angeles Basin, in K. T. Biddle, ed., Active margin basins: AAPG Memoir 52, p. 35–134.

Wernicke, B., G. J. Axen, and J. I. Snow, 1988, Basin and Range extensional tectonics at the latitude of Las Vegas, Nevada, Geol. Soc. Am. Bull.,100, 1738-1757.

Yan, Z., and R. W. Clayton, 2007, Regional mapping of the crustal structure in southern California from receiver functions, J. Geophys. Res., 112, B05311, doi:10.1029/2006JB004622.

Yang, W., E. Hauksson and P. M. Shearer, Computing a large refined catalog of focal mechanisms for southern California (1981 - 2010): Temporal Stability of the Style of

Faulting, *Bull. Seismol. Soc. Am.*, June 2012, v. 102, p. 1179-1194, doi:10.1785/0120110311, 2012.

Yeats, R. S., 1988, Late Quaternary slip rate on the Oak Ridge fault, Transverse Ranges, California, Implications for seismic risk: Journal of Geophysical Research, v. 93, p. 12,137-12,159.

Yeats, R. S., Huftile, G. J., and Grigsby, F. B., 1988, Oak Ridge fault, Ventura fold belt, and the Sisar decollement, Ventura basin, California: Geology, v. 16, p. 1113-1116.

Yerkes, R. F., A. M. Sarna-Wojcicki, and K. R. Lajoie, 1987, Geology and Quaternary deformation of the Ventura area. In: Recent Reverse Faulting in the Transverse Ranges. U.S. Geological Survey Professional Paper 1339, pp. 169–178.

Zhao, L., T. H. Jordan & C. H. Chapman, 2000, Three-dimensional Fréchet differential kernels for seismic delay times, Geophys. J. Int., 141, 58–576; Zhao, L., T. H. Jordan, K. B.

Zoback, M. D., Zoback, M. L., Mount, V. S., Suppe, J., Eaton, J. P., Healy, J. H., Oppenheimer, D., Rosenberg, P., Jones, L., Raleigh, C. B., Wong, I. G., Scotti, O., and Wentworth, C., 1987, New Evidence on the state of stress of the San Andreas fault system: Science, v. 238, p. 1115-1112.

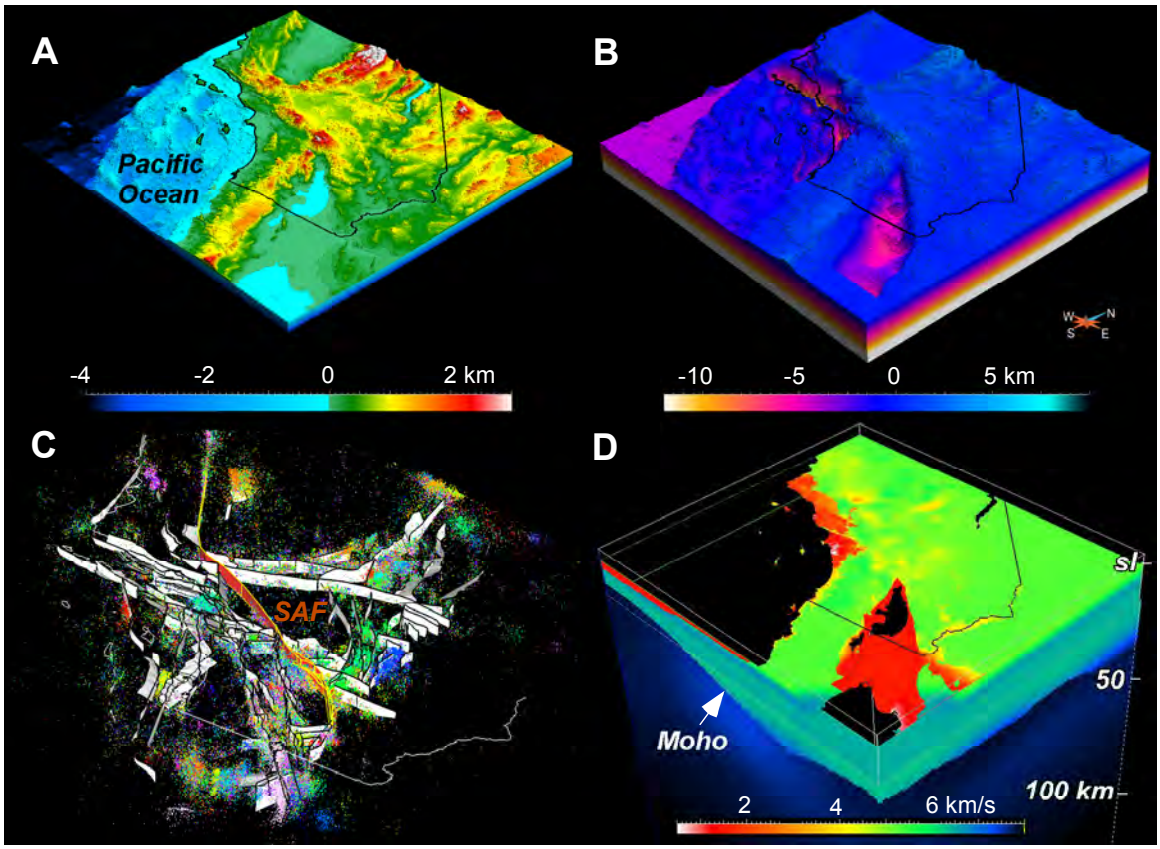
A
Pacific
Ocean
-4
-2
0
2 km
B
-10
-5
0
5 km
C
SAF
D
sl
50
Moho
2
4
6 km/s
100 km

Fig. 1

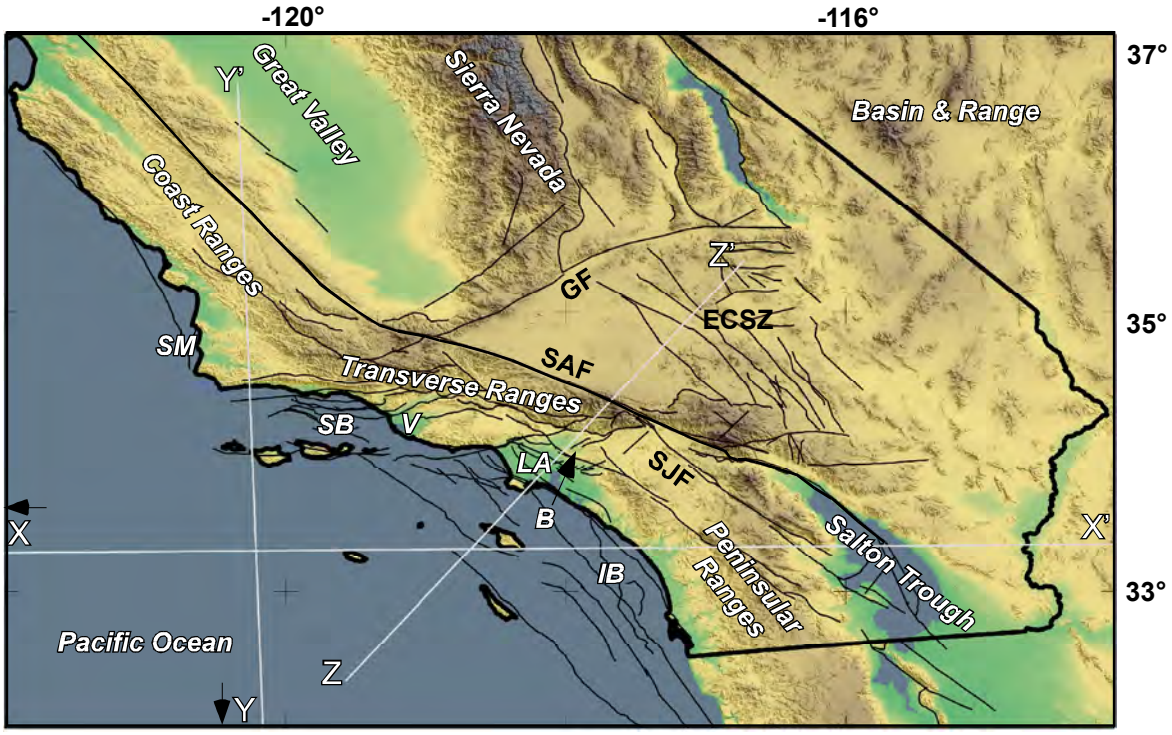
-120°
-116°
37°
35°
33°
Y'
Great Valley
Sierra Nevada
Basin & Range
Coast Ranges
Z'
GF
ECSZ
SM
SAF
Transverse Ranges
SB
V
LA
SJF
X
B
X'
Salton Trough
Peninsular Ranges
IB
Pacific Ocean
Z
Y

Fig. 2

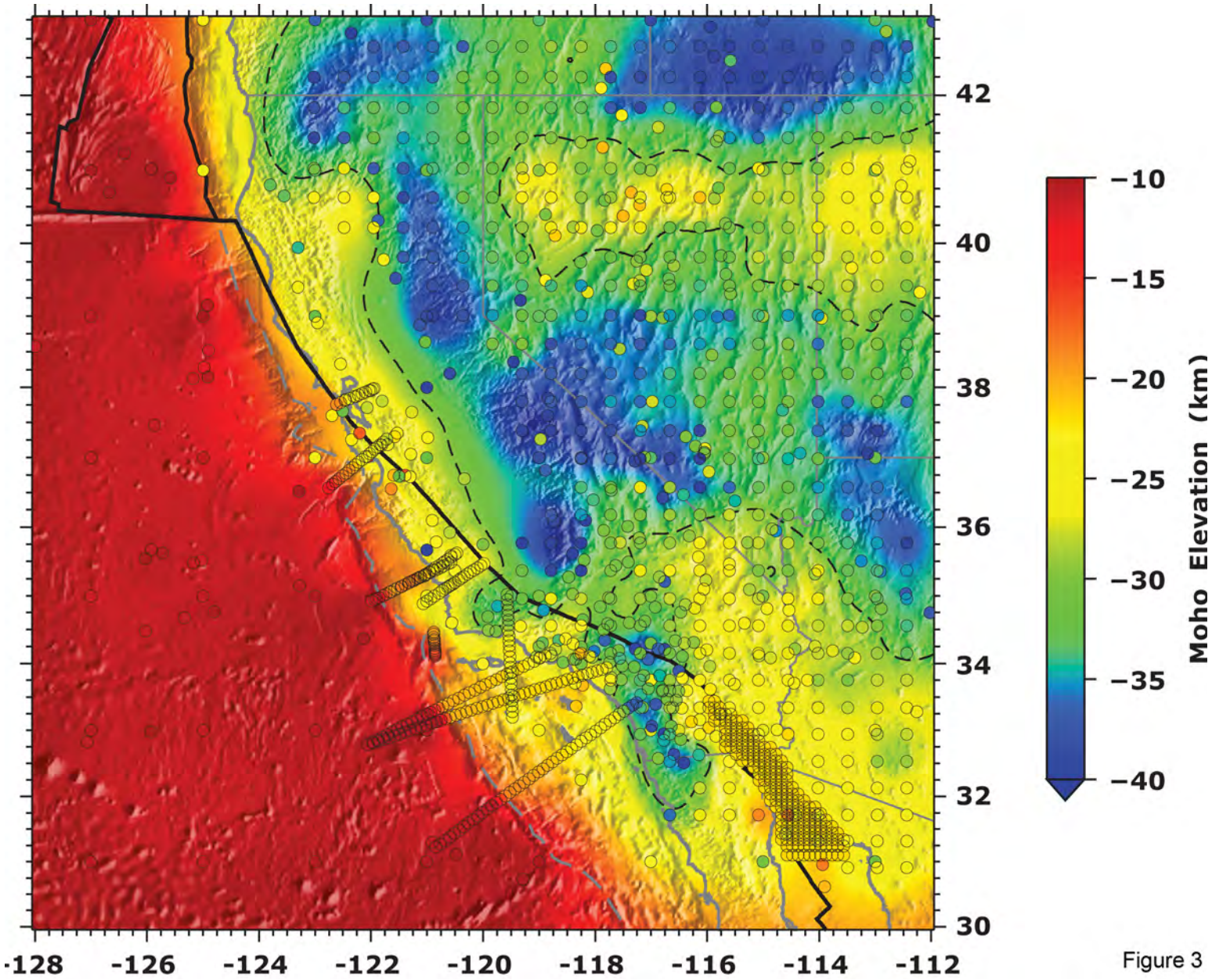
42
40
38
36
34
32
30
-128
-126
-124
-122
-120
-118
-116
-114
-112
-10
-15
-20
-25
-30
-35
-40
Moho Elevation (km)

Figure 3

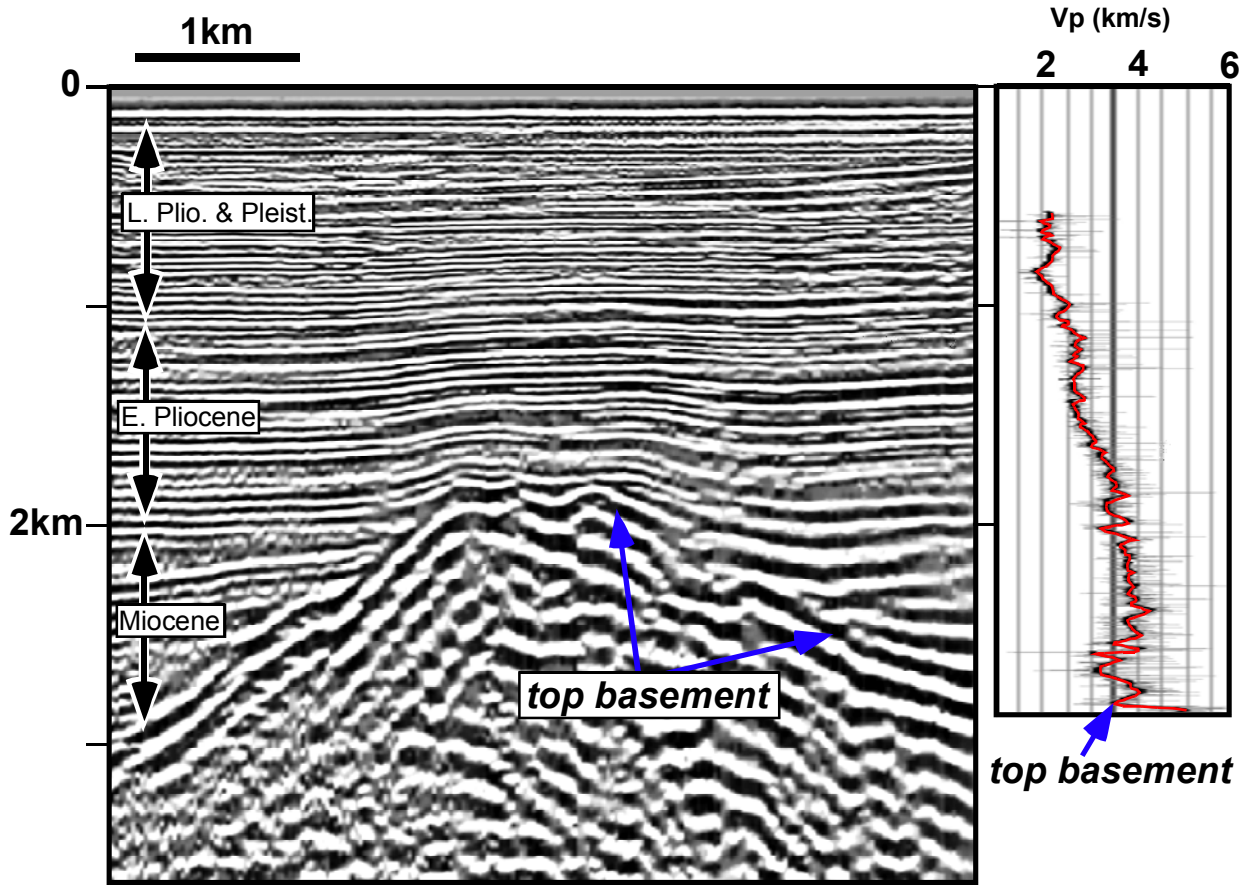
1km
0
2km
L. Plio. & Pleist.
E. Pliocene
Miocene
top basement
Vp (km/s)
2
4
6
top basement

Fig. 4

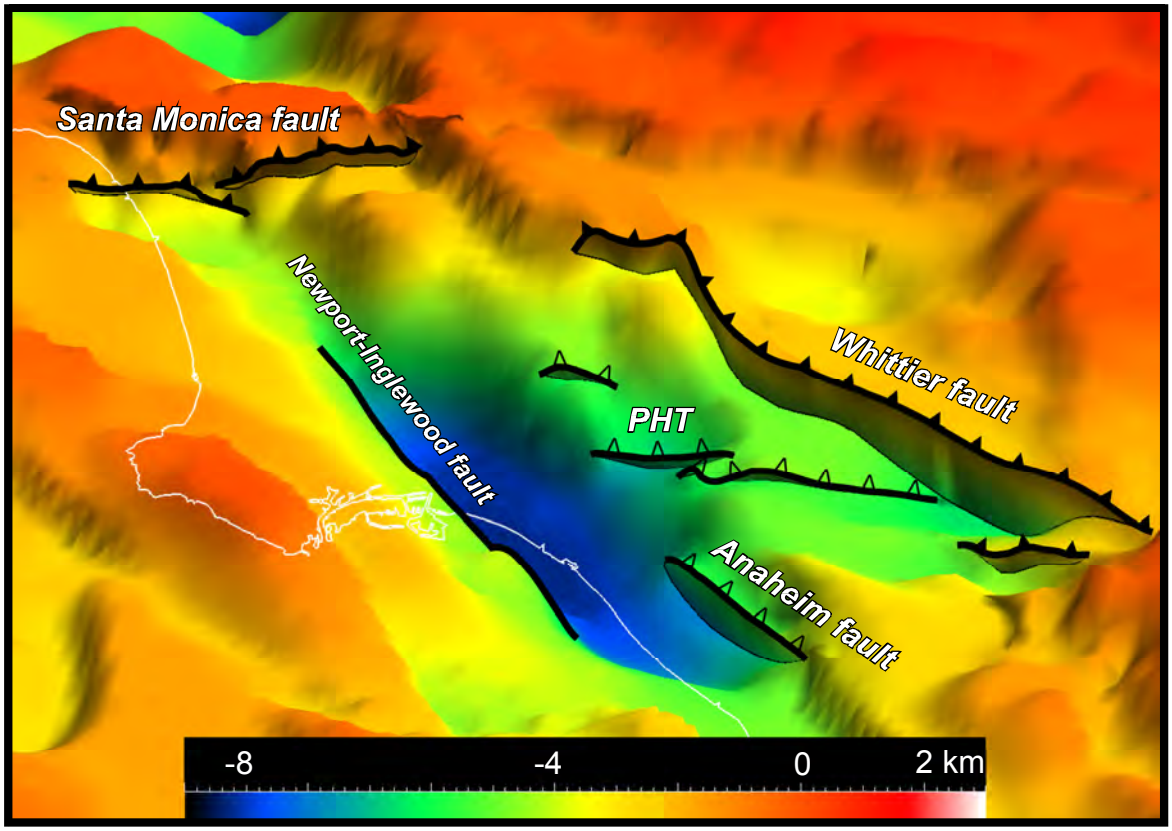
Santa Monica fault
Newport-Inglewood fault
PHT
Whittier fault
Anaheim fault
-8
-4
0
2 km

Fig. 5

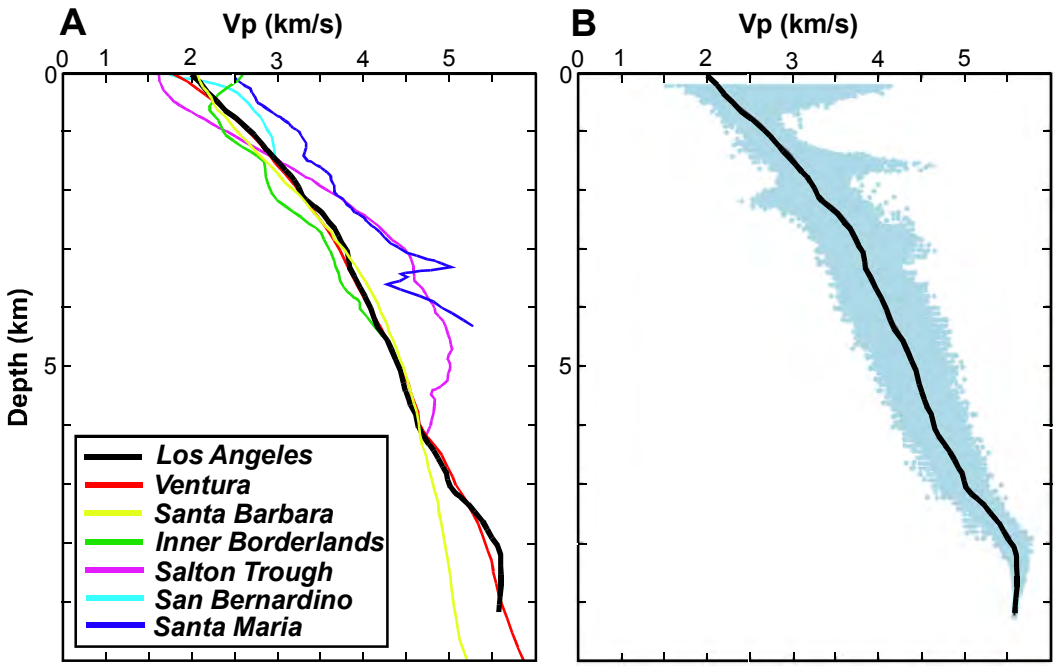
A
Vp (km/s)
0
1
2
3
4
5
Depth (km)
Los Angeles
Ventura
Santa Barbara
Inner Borderlands
Salton Trough
San Bernardino
Santa Maria
B
Vp (km/s)

Fig. 6

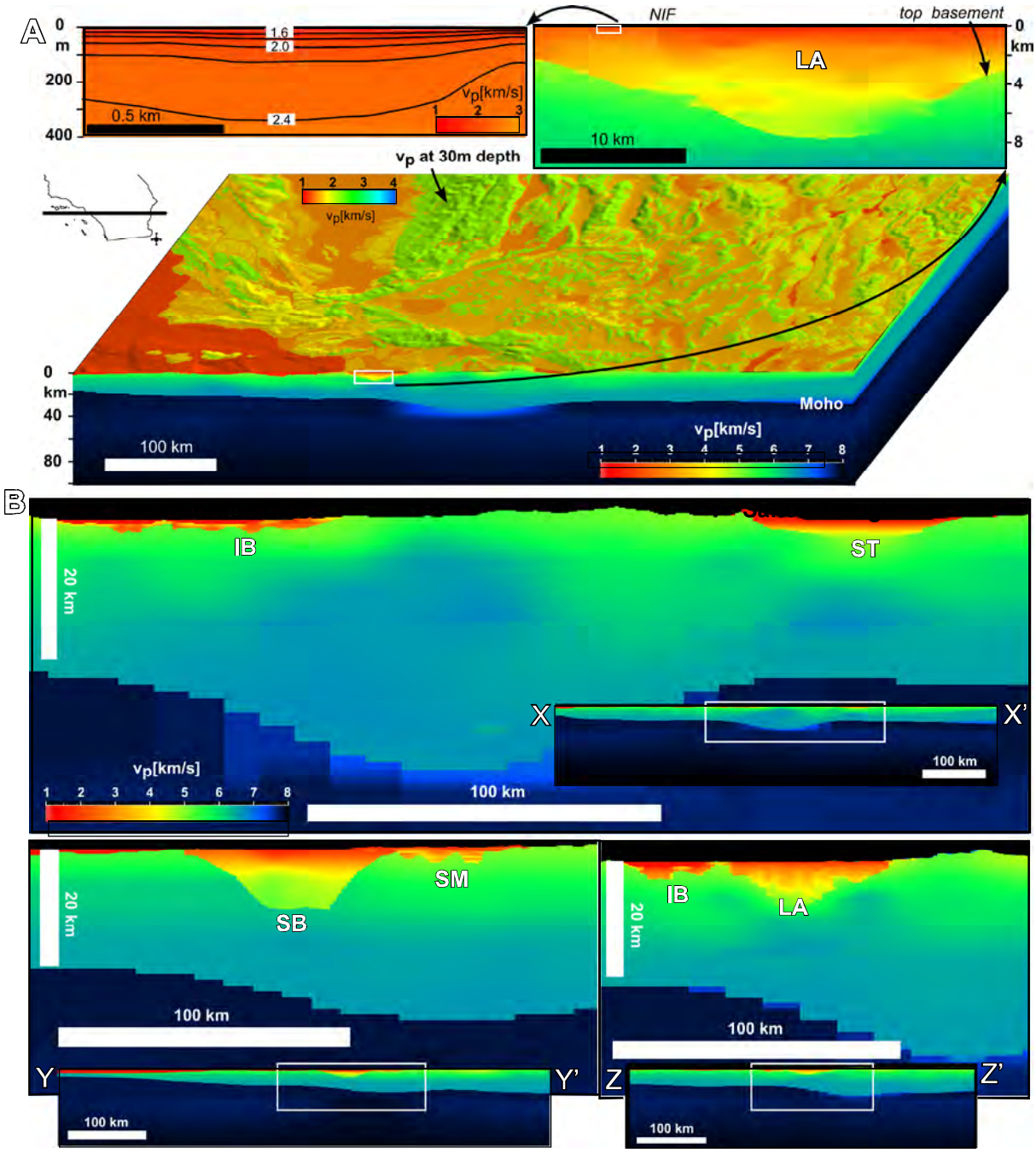
A
0
m
200
400
1.6
2.0
2.4
0.5 km
vp[km/s]
1
2
3
NIF
top basement
LA
0
km
4
8
10 km
vp at 30m depth
1 2 3 4
vp[km/s]
0
km
40
80
100 km
Moho
vp[km/s]
1 2 3 4 5 6 7 8
B
IB
ST
20 km
X
X'
100 km
vp[km/s]
1 2 3 4 5 6 7 8
100 km
SM
SB
20 km
100 km
Y
Y'
100 km
IB
LA
20 km
100 km
Z
Z'
100 km

Fig. 7

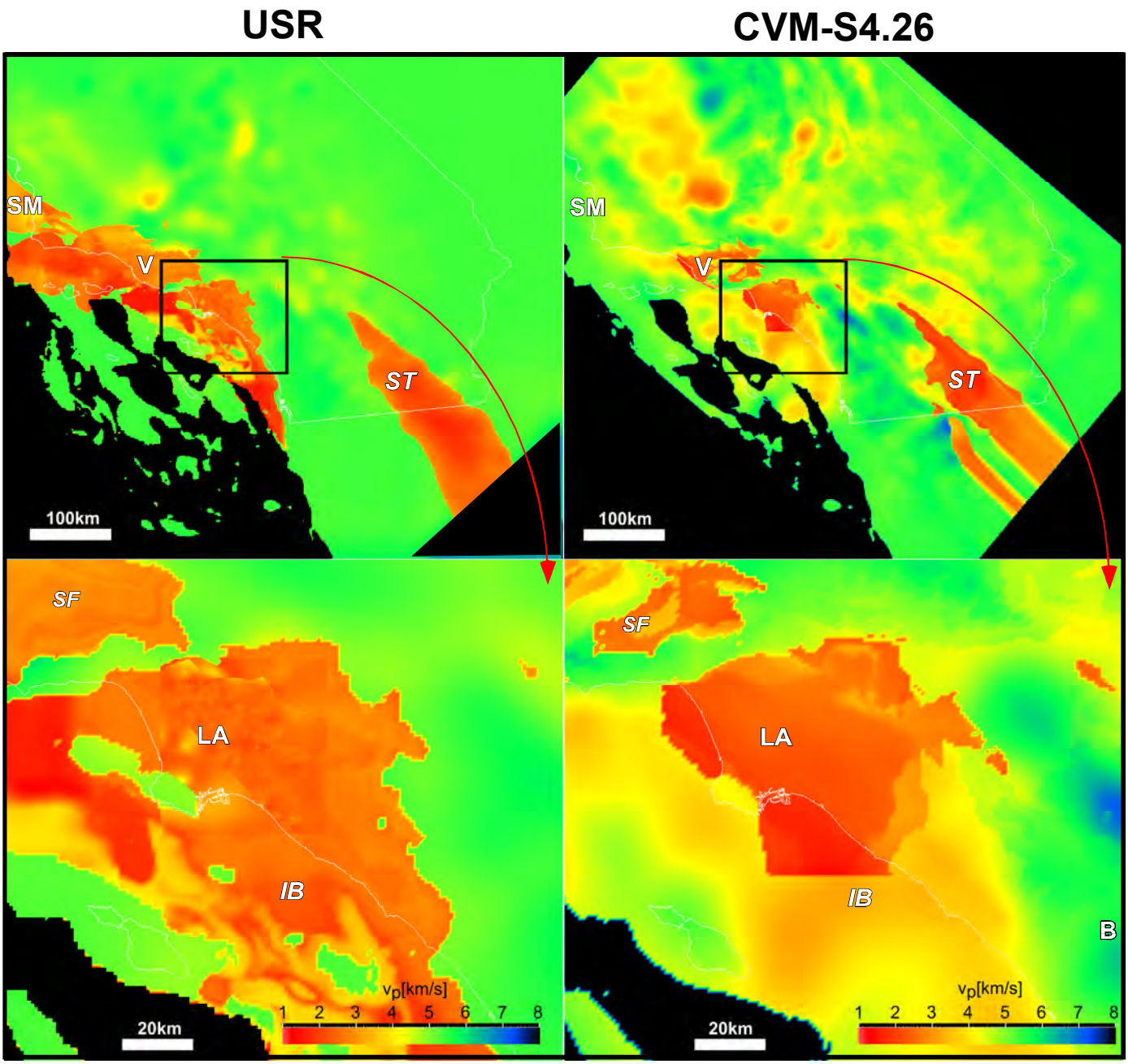


Fig. 8

(a) Mw 7.9 scenario thrust earthquake

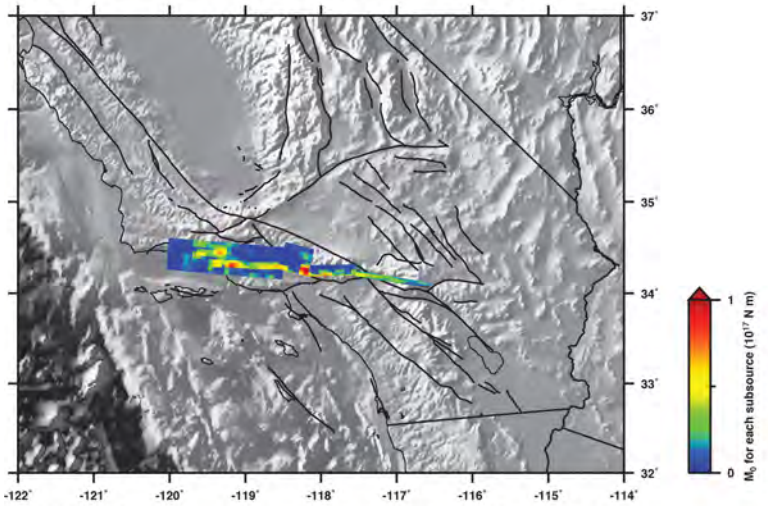


(b) Peak ground velocity using SoCal-1D

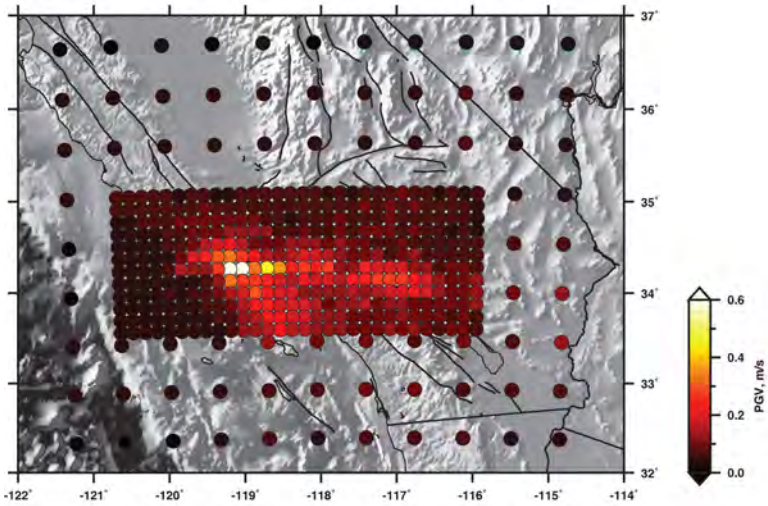


(c) Peak ground velocity using CVM-H

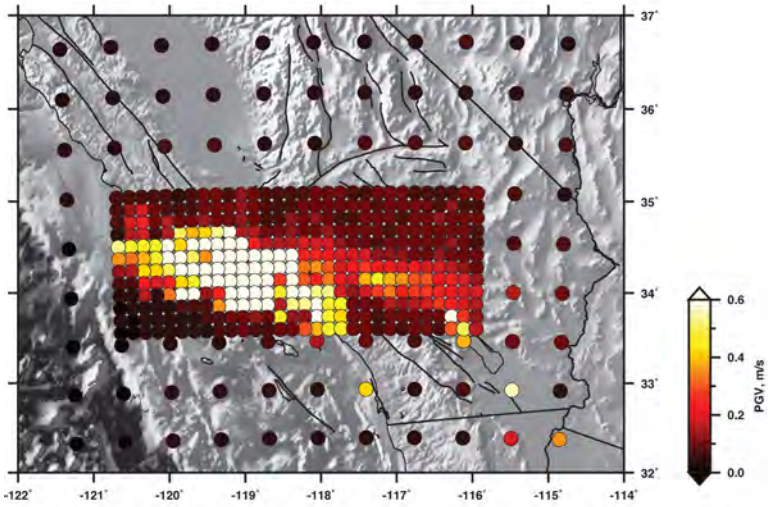


Figure 9

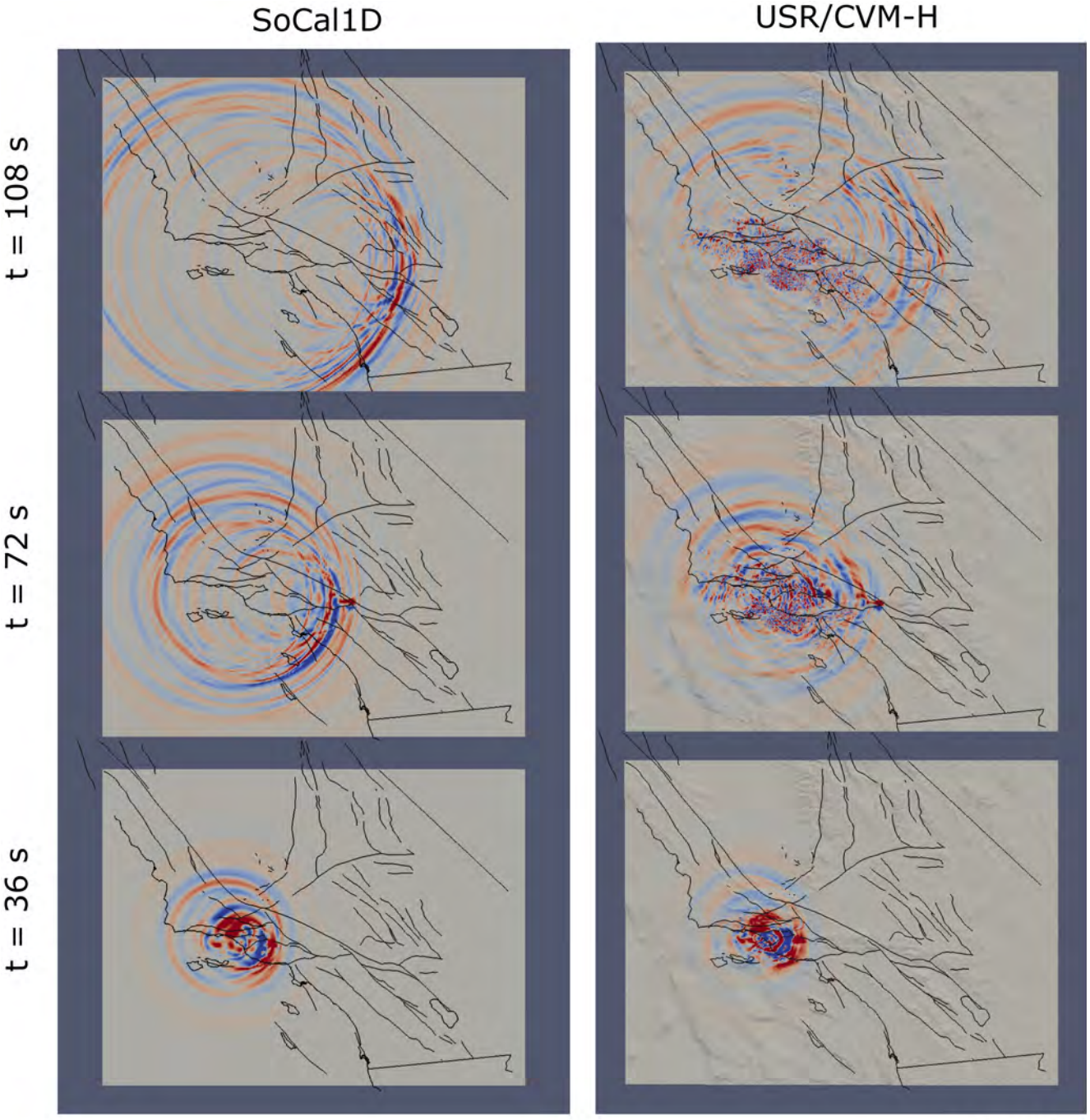


Figure 10

Supplementary Material for

# Unified Structural Representation of the southern California crust and upper mantle

John H. Shaw, Andreas Plesch, Carl Tape, M. Peter Suess, Thomas H. Jordan, Geoffrey Ely, Egill Hauksson, Jeroen Tromp, Toshiro Tanimoto, Robert Graves, Kim Olsen, Craig Nicholson, Phil Maechling, Carlos Rivero, Peter Lovely, Charles M. Brankman, Jason Munster

*Earth and Planetary Science Letters*
January 13, 2015

## S1 GTL parameterization

The GTL implemented in the USR was based on *Ely et al.* (2010) and uses the geology-based Vs30 maps of *Wills and Clahan* (2006) to specify velocity values at the Earths surface in the voxet. $V_P$, and in turn density, are inferred from surface $V_S$ using the scaling laws of *Brocher* (2005). These values were parameterized to a depth of $z_T = 350$ meters with the following formulations:

$$V_S(z) = f(z)V_{ST} + g(z)V_{S30} \quad \text{(S1)}$$

$$V_P(z) = f(z)V_{PT} + g(z)P(V_{S30}), \quad \text{(S2)}$$

where $z'$ is depth, $V_{ST}$ and $V_{PT}$ are are S- and P-wave velocities extracted from the crustal velocity model at depth $z_T$, $P()$ is the *Brocher* (2005) P-wave velocity scaling law, and

$$z = z'/z_T \quad \text{(S3)}$$

$$f(z) = z + b(z - z^2) \quad \text{(S4)}$$

$$g(z) = a - az + c(z^2 + 2z - 3z) \quad \text{(S5)}$$

The coefficient $a$ controls the ratio of surface velocity to original 30 meter average, $b$ controls overall curvature, and $c$ controls near-surface curvature of the velocity profile. The coefficients $a = 1/2$, $b = 2/3$, and $c = 3/2$ were chosen to fit the generic rock profile of *Boore and Joyner* (1997) while also producing smooth and well-behaved profiles when combined with the underlying basin and crustal velocity models (*Ely et al.*, 2010) (Figure 7).

## S2 Model validation, comparison, and uncertainty

The velocity model (CVM) component of the USR described here is assembled from several different data sets and models, and thus it is challenging to formally assess model resolution and uncertainties. One clear step for the sedimentary basins is to assess the variability in well data that is not represented in the final model. As we discussed, these data measure interval transit times over borehole distances of less than 1 m, whereas the velocity model uses smoothed (25 m sampled) versions of these data. To make this assessment, we compared observations directly with the velocity values represented at 108 well bore locations in the Los Angeles basin. Our analysis shows a standard deviation of 6.5% around a mean of 1.0 for the ratio between compressional wave slowness in logs and the model in a population of ca. 1.1 million samples. This corresponds to a standard deviation in $V_P$ of $\pm$99 m/s at 2000 m/s.

For general descriptions of resolution of the crust and mantle velocity representations, readers are referred to *Hauksson* (2000), *Tape et al.* (2009, 2010), and *Prindle and Tanimoto* (2006). Given that the USR described here is assembled from several different data sets and models, not from any single inversion, there is no formal assessment of resolution. There are, however, several possibilities for evaluating complex seismic velocity models such as the CVM. We review them here in order to highlight some possible future directions, as well as to demonstrate some of the challenges that arise from constructing a model from many different data sets across different scales. Any seismic velocity model could be interrogated with a wide range of different data sets, such as gravity data, teleseismic data (e.g., receiver functions), ambient-noise cross correlations, regional earthquake data, wide-angle seismic refraction data, and seismic reflection data. The basic approach is to compare the synthetic wavefield predicted by the model with the observed wavefield, by formally evaluating some measure of misfit. For such comparisons, a key choice is the frequency content of the seismic data; filtering at higher frequencies will decrease the quality of predictive capability of the velocity model. Much of the data used in the CVM are from well logs that provide direct measurements of $V_P$ within the sedimentary basins. However, most regions of southern California could be evaluated by comparing wavefield predictions from CVM with the observed wavefield for regional earthquakes that were not used in constructing the crustal model (*Tape et al.*, 2009).

Model comparisons can be made either by comparing seismic velocities between two models or by comparing misfit measures for two models, whereby an independent set of observations is used to evaluate the misfit for each model. The recent study of *Lee et al.* (2014a,b) provides comparisons between a previous version of the model described here and a new iteration of their model. Their comparison was made for regional earthquakes for periods of 5!s and longer and provides a quantitative evaluation of the longer length scale features, especially for $V_S$, in the CVM.

A comprehensive estimation of uncertainties associated with large and complex models such as CVM is not currently tenable due to computational limitations. Uncertainties could be obtained by separately perturbing each grid point within the CVM and then evaluate the change in misfit due to the perturbation. This would require having as large a set of reference data as possible, spanning from the well log scale to the crustal and mantle scales. Certain gridpoints could be perturbed a lot without impacting the misfit; these grid points would have large uncertainties. Other gridpoints, such as those constrained by well logs, could not be perturbed much; these would have small uncertainties. Some information on uncertainties could be obtained with fewer simulations by perturbing the entire model with Gaussian random fields to evaluate how the strength and length scale of the perturbations affect the misfit assessment. The resolution of a model is a characterization of the length scales of features that can be reliably determined within a formal tomographic inversion. The classical model used in seismology for resolution tests are checkerboard patterns (in 2D and 3D). These tests have been performed for 3D reference models (*Chen et al.*, 2007; *Lee et al.*, 2014a,b); however, for gradient-based methods the computational cost of the resolution test is comparable to the inversion itself (*Fichtner et al.*, 2009).

## References


Boore, D. M., and W. B. Joyner (1997), Site amplifications for generic rock sites, *Bull. Seis. Soc. Am.*, *87*(2), 327–341.

Brocher, T. M. (2005), Empirical relations between elastic wavespeeds and density in the Earth's crust, *Bull. Seis. Soc. Am.*, *95*(6), 2081–2092.

Chen, P., L. Zhao, and T. H. Jordan (2007), Full 3D tomography for the crustal structure of the Los Angeles region, *Bull. Seis. Soc. Am.*, *97*(4), 1094–1120.

Ely, G., T. H. Jordan, P. Small, and P. J. Maechling (2010), A $V_{S30}$-derived near-surface seismic velocity model, Abstract S51A-1907 presented at 2010 Fall Meeting, AGU, San Francisco, Calif., 13-17 Dec.

Fichtner, A., B. L. N. Kennett, H. Igel, and H.-P. Bunge (2009), Full seismic waveform tomography for upper-mantle structure in the Australasian region using adjoint methods, *Geophys. J. Int.*, *179*, 1703–1725.

Hauksson, E. (2000), Crustal structure and seismicity distribution adjacent to the Pacific and North America plate boundary in southern California, *J. Geophys. Res.*, *105*(B6), 13,875–13,903.

Lee, E.-J., P. Chen, T. H. Jordan, P. B. Maechling, M. A. M. Denolle, and G. C. Beroza (2014a), Full-3-D tomography for crustal structure in Southern California based on the scattering-integral and the adjoint-wavefield methods , *J. Geophys. Res. Solid Earth*, *119*, 6421–6451, doi:10.1002/2014JB011346.

Lee, E.-J., P. Chen, and T. H. Jordan (2014b), Testing waveform predictions of 3D velocity models against two recent Los Angeles earthquakes, *Seis. Res. Lett.*, *85*(6), 1275–1284.

Prindle, K., and T. Tanimoto (2006), Teleseismic surface wave study for S-wave velocity structure under an array: Southern California, *Geophys. J. Int.*, *166*, 601–621.

Tape, C., Q. Liu, A. Maggi, and J. Tromp (2009), Adjoint tomography of the southern California crust, *Science*, *325*, 988–992.

Tape, C., Q. Liu, A. Maggi, and J. Tromp (2010), Seismic tomography of the southern California crust based on spectral-element and adjoint methods, *Geophys. J. Int.*, *180*, 433–462.

Wills, C. J., and K. B. Clahan (2006), Developing a map of geologically defined stie-condition categories for California, *Bull. Seis. Soc. Am.*, *96*(4A), 1483–1501.